Modeling of a Magnetic Coupler Based on Single- and Double-Layered Rectangular Planar Coils With In-Plane Misalignment for Wireless Power Transfer

Francisco Javier López-Alcolea, *Member, IEEE*, Javier Vázquez del Real, Pedro Roncero-Sánchez, *Senior Member, IEEE*, and Alfonso Parreño Torres

***Abstract*—This article proposes an analytical model that provides accurate self-inductance and mutual inductance calculations for two mutually coupled rectangular, planar, and spiral coils with an air core, which are equal and parallel, including the possibility of a lateral misalignment. Both single- and double-layered coil geometries were modeled by considering an arbitrary number of turns with a circular cross section per layer. The model equations, which can be readily implemented in software, are the results of a systematic approach that starts from the equations for the self-inductance of a wire and the mutual inductance of two parallel and misaligned wires that lie on the same plane. Accuracy is guaranteed by considering all the magnetic interactions among the individual turns in the two coils, while the simplifications involve only the calculations made at the corners of the coils. The model was validated by taking as reference experimental measurements carried out on a rectangular and a square magnetic coupler. A second analytical model, based on equivalent single-turn coils, was also tested for comparison purposes. The validation was extended with finite-element analysis tools by considering a wide range of coil side lengths, air gaps, number of turns, and lateral misalignments. The proposed model can, therefore, be regarded as a reliable tool to aid in the design of rectangular-shaped air-core magnetic couplers with applications in the contactless transfer power that are not necessarily limited to vehicle electrification.**

***Index Terms*—Analytical model, electric vehicle (EV), inductive coupling, magnetic coupler, misalignment, mutual inductance, rectangular coils, self-inductance, wireless power transfer.**

I. Introduction

INDUCTIVE power transfer (IPT) has, in recent years, become an increasingly popular wireless technology for the recharging of a wide range of electrical battery-powered goods. A large variety of IPT systems have been developed for a number of diverse branches of industry, such as consumer electronics, biomedical devices, LED lighting, robotics, or electric vehicles (EVs) [1]–[5]. In the case of the automotive sector, the increase in greenhouse gas emissions and the depletion of fossil fuels are causing a growing interest in the development of EVs.

Although the only technology that was initially available for the battery charging of EVs was limited to wired chargers, inductive charging, which is characterized by a galvanic isolation between the user and the charger, is gradually taking place owing to a safer and more comfortable charging environment [6]–[8].

The operating principle of an IPT system is based on the coupling of magnetic flux between the two windings of a contactless magnetic coupler when they are sufficiently close to each other. The magnetic coupler design can be aided by a combination of purely analytical formulations and finite-element analysis (FEA) software tools. In the case of air-core magnetic couplers, the design is sometimes carried out using only analytical models. However, ferrite cores and even aluminum plates are sometimes part of the magnetic coupler, in an attempt to boost the fraction of the magnetic flux that is linked to the secondary side while shielding the magnetic field. Sophisticated magnetic couplers of this type have been reported in some high-efficiency IPT designs for EV chargers in recent years. Unfortunately, in these cases, proposing analytical methods for designing couplers becomes significantly more complex, and consequently, such analytical approaches are usually replaced with FEA models [9], [10]. Note, however, that purely analytical methods can still play a significant role, at least in the early design stages of magnetic couplers, even for EV applications: in spite of the computational power and the reliability that are characteristic of advanced FEA tools, it should be pointed out that the numerous modifications undergone by a given FEA model during the iterative design process of a physical system are normally user-intensive, since the model needs to be constantly updated. On the contrary, if the magnetic coupler design relies on a sound analytical formulation whose equations can be implemented in software, not only are the results equally reliable, but also any change in the design parameters implies little effort for the user.

A number of previous works describe a variety of approaches whose objective is to determine both the self-inductances and the

Manuscript received January 24, 2019; revised April 19, 2019 and July 31, 2019; accepted September 14, 2019. Date of publication September 26, 2019; date of current version February 11, 2020. This work was supported in part by the Ministry of Economy and Competitiveness of Spain and in part by the European Regional Development Fund under the Research Project ENE2015-71417-R (MINECO/FEDER, UE). Recommended for publication by Associate Editor O. C. Onar. *(Corresponding author: Francisco Javier López-Alcolea.)*

F. J. López-Alcolea, J. V. del Real, and P. Roncero-Sánchez are with the Institute of Energy Research and Industrial Applications, University of Castilla–La Mancha, 13071 Ciudad Real, Spain (e-mail: FJavier.Lopez@uclm.es; Javier.Vazquez@uclm.es; pedro.roncero@uclm.es).

A. P. Torres is with the Institute of Industrial Development, Castilla–La Mancha Science and Technology Park, 02001 Albacete, Spain (e-mail: alfonso.parreno@pctclm.com).

Color versions of one or more of the figures in this article are available online at http://ieeexplore.ieee.org.

Digital Object Identifier 10.1109/TPEL.2019.2944194

mutual inductance of a pair of mutually coupled coils. Several simplified self-inductance calculations for coils featuring various geometries were provided by Thomson [11], while Wheeler proposed equations for circular and square coils based on elliptical integrals [12]. In the work by Hurley *et al.*, numerical methods were applied in order to solve an integral formula [13], while Bueno and Assis proved the equivalence of the formulations developed by Neumann, Weber, Maxwell, and Graneau as regards solving the self-inductance of a closed circuit [14] and also proposed a method for inductance calculations [15]. The analysis carried out by Luo and Wei employed the Fourier–Bessel transformation and the dual Fourier transformation for square and circular coils [16], while Grover presented a set of equations adapted to work with tabular data, along with some formulae that rely solely on the geometrical features of the coils [17]. The issue of misalignment between coils has already been addressed by some authors, such as Dehui *et al.*, who focused on the modeling of the mutual coupling between rectangular spiral coils with lateral misalignment in air [18], or Raju *et al.* who approached the problem of the misalignment between square coils by assuming that they are circles with scaled diameters [19]. Soma *et al.* developed expressions based on elliptic integrals considering two circular coils with planar and angular misalignments [20]. Fotopoulou and Flynn provided analytical expressions for the efficiency, avoiding the treatment of the mutual inductance and considering lateral and angular misalignments [21].

This article proposes an accurate analytical model, whose purpose is to perform inductance calculations on a magnetic coupler composed of two magnetically coupled rectangular, planar, and spiral coils that are wound with wire of a circular cross section. The influence of extra elements added to the magnetic coupler such as aluminum shields or ferrite plates is, therefore, out of the scope of the proposed model. The model, which was developed for single- and double-layer coils that are equal and parallel, results in practical expressions for both the self-inductance and the mutual inductance, in addition to covering the case of in-plane misalignment. The approach chosen to build the model was, on the one hand, inspired by some of Rosa and Grover's early works that derived analytical expressions for the self-inductance and the mutual inductance of single-turn square and rectangular ideal circuits [22], [23]. It was, on the other hand, inspired by the self-inductance calculations made by Greenhouse [24] for spiral and planar coils featuring multiple turns. The case of angular misalignment was ruled out, since the starting equations from which the model was built are not suitable to simultaneously consider lateral and angular misalignments. One of the main advantages of the proposed model equations is that they can be easily programmed in a high-level programming language, as opposed to certain other formulas reported in the literature that involve awkward integral expressions. This was accomplished by taking as a starting point the basic equations that yield the self-inductance of a straight wire and the mutual inductance of two equal, parallel, and misaligned wires located on the same plane. Considering that each turn in either of the two rectangular coils can be split into four straight wires joined by their edges, the model takes into account every single interaction between a given straight wire in one of the two rectangular coils and the remaining wires in both coils. Simplifications involve only the calculations performed on the corners of the coils, thus contributing to the accuracy of the final equations. A further advantage of the model is that it yields analytical expressions that involve only geometrical parameters of the magnetic coupler, signifying that it can be useful in any IPT design, regardless of its size.

The initial equations on which the proposed model is built are presented in Section II. The expressions for the self-inductance of a rectangular single-layer coil and for the mutual inductance of two mutually coupled, equal, and coaxial single-layer coils are thoroughly derived in Section III, whereas the extension to double-layer coils follows in Section IV. Section V is devoted to the generalization of the model in order to include the case of in-plane misalignment for rectangular single-layer coils. A simplified analytical approach based on the reduction of a square coil to an equivalent single-turn coil is then described in Section VI in order to compare it with the proposed model. A setup of the FEA tool is described in Section VII. The degree of accuracy attained by both analytical models is assessed in Section VIII by using experimental and FEA results. The performance of the proposed model with different coil arrangements is assessed in Section IX, while a summary of its strengths is outlined in Section X. Section XI gives the conclusion.

II. Initial Equations for L and M

The two initial equations from which the model is built yield the self-inductance of a straight conductor and the mutual inductance of two equal and parallel straight filaments that lie on the same plane and are misaligned, assuming in both cases that the cross-sectional area of the wires is circular and that the surrounding medium is the free space. The change in the magnetic permeability μ is negligible if the medium is air rather than a vacuum. SI units will be used throughout the formulation.

The self-inductance L of a straight round copper wire of length l and radius ρ, either in a vacuum with a magnetic permeability μ_0 or in air, is given by [22], [23]

$$L(l,\rho)=\frac{\mu_0}{4\pi}2\left[l\cdot\ln\left(\frac{l+\sqrt{l^2+\rho^2}}{\rho}\right)-\sqrt{l^2+\rho^2}+\frac{l}{4}+\rho\right]. \quad (1)$$

In turn, the mutual inductance M for the general case, in which two straight conductors of lengths l and m lie on the same plane, are a distance d apart, and are displaced from each other by a distance Δ, as shown in Fig. 1, obeys the following expression [23]:

$$\begin{aligned}M=\frac{\mu_0}{4\pi}\Bigg[&\alpha\sinh^{-1}\left(\frac{\alpha}{d}\right)-\beta\sinh^{-1}\left(\frac{\beta}{d}\right)\\&-\gamma\sinh^{-1}\left(\frac{\gamma}{d}\right)+\Delta\sinh^{-1}\left(\frac{\Delta}{d}\right)\\&-\sqrt{\alpha^2+d^2}+\sqrt{\beta^2+d^2}\\&+\sqrt{\gamma^2+d^2}-\sqrt{\Delta^2+d^2}\Bigg]\end{aligned} \quad (2)$$

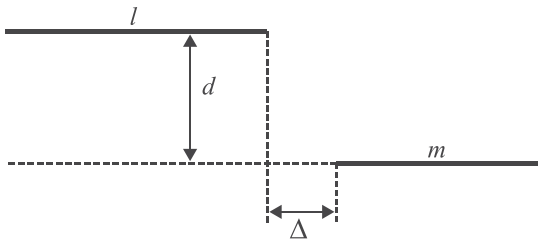

Fig. 1. Geometry of two misaligned conductors that allows their mutual inductance M to be calculated.

where

$$\begin{aligned}\alpha &= l + m + \Delta \\ \beta &= l + \Delta \\ \gamma &= m + \Delta.\end{aligned} \tag{3}$$

Note that (1) and (2) are strictly valid for wires of a circular cross section. For other cross-sectional shapes, (1) is to be replaced with the appropriate expression, whereas (2) can still be applied, provided the separation d is replaced with the geometric mean distance of the cross sections of the conductors [23].

The mutual inductance equation when the cross section of the coil is small compared with its length (which covers the majority of cases) are sensibly the same as those of their central filaments.

If both filaments are of equal length l, which is the case of interest for the proposed model, the parameters α, β, and γ become

$$\begin{aligned}\alpha &= 2l + \Delta \\ \beta &= \gamma = l + \Delta.\end{aligned} \tag{4}$$

By using (4), (2) adopts the following simplified form:

$$\begin{aligned}M_\Delta(l,d,\Delta) = \frac{\mu_0}{4\pi}\Bigg[&\alpha \sinh^{-1}\left(\frac{\alpha}{d}\right) - 2\beta \sinh^{-1}\left(\frac{\beta}{d}\right) \\ &+ \Delta \sinh^{-1}\left(\frac{\Delta}{d}\right) - \sqrt{\alpha^2+d^2} \\ &+ 2\sqrt{\beta^2+d^2} - \sqrt{\Delta^2+d^2}\Bigg].\end{aligned} \tag{5}$$

In the particular case of filaments that are not only equal, but are also perfectly aligned with each other (that is, $\Delta = -l$), α, β, and γ are

$$\begin{aligned}\alpha &= l \\ \beta &= \gamma = 0.\end{aligned} \tag{6}$$

In this case, (5) is further simplified to

$$M(l,d) = \frac{\mu_0}{4\pi} 2\left[l \cdot \sinh^{-1}\left(\frac{l}{d}\right) - \sqrt{l^2+d^2} + d\right]. \tag{7}$$

By using

$$\sinh^{-1}(x) = \ln\left(x + \sqrt{x^2+1}\right) \tag{8}$$

(5) and (7) can be expressed in logarithmic form as follows:

$$\begin{aligned}M_\Delta(l,d,\Delta) = \frac{\mu_0}{4\pi}\Bigg[&\alpha \ln\left(\frac{\alpha+\sqrt{\alpha^2+d^2}}{d}\right) - \sqrt{\alpha^2+d^2} \\ &- 2\beta \ln\left(\frac{\beta+\sqrt{\beta^2+d^2}}{d}\right) + 2\sqrt{\beta^2+d^2} \\ &+ \Delta \ln\left(\frac{\Delta+\sqrt{\Delta^2+d^2}}{d}\right) - \sqrt{\Delta^2+d^2}\Bigg]\end{aligned} \tag{9}$$

$$M(l,d) = \frac{\mu_0}{4\pi} 2\left[l \cdot \ln\left(\frac{l+\sqrt{l^2+d^2}}{d}\right) - \sqrt{l^2+d^2} + d\right]. \tag{10}$$

III. Modeling of Two Single-Layer Coupled Coils

This section describes the formulation that results in the model equations for the self-inductance of a single-layer rectangular coil and the mutual inductance of two single-layer rectangular coils that are equal, coaxial, and parallel.

The major assumptions observed during the modeling are listed as follows.

1) The medium in which the coils are placed is air, so the magnetic permeability of the medium corresponds with that of the vacuum, μ_0.
2) The two coils have the same shape and size.
3) All the wires in a given coil side have the same averaged length for the calculation of the mutual inductance.
4) The cross-sectional area of the coil wire is circular.
5) The current flowing through a cross-sectional area of the coil is uniformly distributed.
6) The operating frequency of the IPT system is well below the self-resonant frequency of the coil.

The uniform current distribution over the cross section of the wire can be ensured by the use of Litz wire with a strand radius smaller than the current penetration at the frequency of operation. Furthermore, the insulation around every single strand in the wire narrows down the current displacements to the cross sections of the individual strands, which are always very small in this kind of wire. Therefore, the influence of external fields on the current distribution is strongly limited when choosing Litz wire. Note that inductance calculations based on high-frequency models would be necessary only in the case of operating the coils at a frequency high enough to have the skin effect play a major role on the current distribution. On the other hand, the assumption that the frequency of operation must be well below the self-resonant frequency of the coils is necessary in order to minimize the influence of the stray capacitance that exists in parallel with the coil inductance on the inductive behavior of an ideal coil. Previous models obtained accurate results in this context, provided that the frequency of operation is kept below half the self-resonant frequency [25].

A. Geometrical Features of the Magnetic Coupler

Considering the shape of vehicles, rectangular-shaped coils are a suitable choice for the magnetic coupler of an IPT system designed for wireless EV charging [6]. Also, Raju *et al.* stated

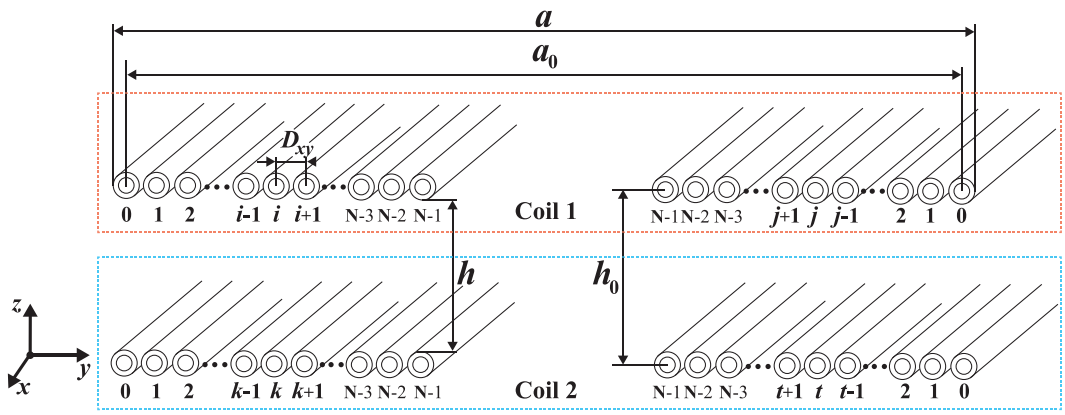

Fig. 2. Cross-sectional view of two equal, coaxial, and parallel single-layer coils with N turns per coil wound with the wire of circular cross section.

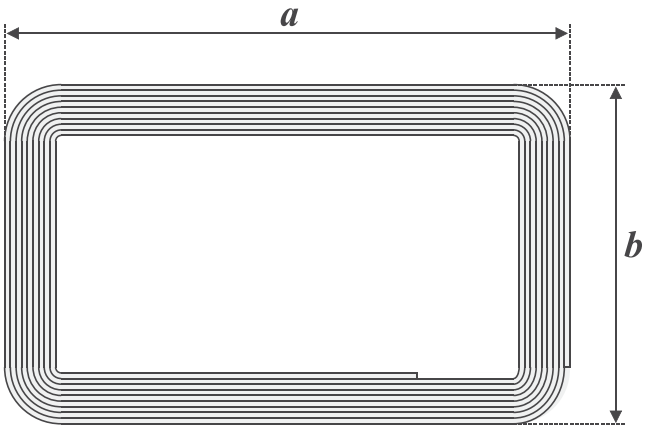

Fig. 3. Top view of a planar, spiral, and rectangular-shaped multiturn coil.

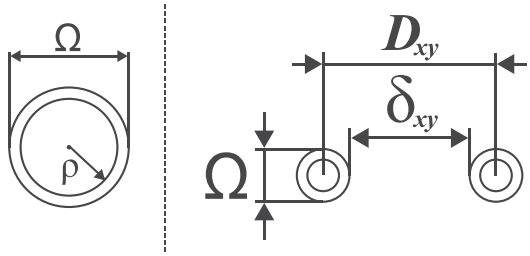

Fig. 4. Definition of the turn gap δ_{xy} and the distance D_{xy} between adjacent wires on the xy plane. Ω and ρ represent the diameter of the wire with and without insulation, respectively.

that the mutual inductance of a square coil is $(4/\pi)^2$ times larger than that of a circular coil inscribed in the square [19]. In addition, Luo and Wei pointed out that the field distribution generated by rectangular coils is more uniform than that of circular coils, which results in a smaller coupling coefficient variation when misalignment occurs [26]. The proposed model applies to two equal, coaxial, and parallel rectangular-shaped coils in air with N turns per layer and outer sides a and b, which are separated by an air gap h, as depicted in Figs. 2 and 3. Note that the first turn has been labeled with 0 rather than 1. This is not an arbitrary choice, since the formulation relies heavily on calculating the distance between individual turns in a number of cases, and the resulting expressions are far simpler when starting the numbering with 0.

The model parameters, a, b, and h can be obtained experimentally, as they are measured from the outer surface of the turns, whereas a_0, b_0, and h_0 are derived from them, as they are all taken from the centers of their corresponding turns. The fact that a, b, and h can be accurately measured on an actual prototype contributes to perform a reliable experimental validation of the model. Equations (11)–(13) show that both sets of parameters relate to each other through the use of Ω, which represents the diameter of the cable, including the insulation and the conduction core

$$a_0 = a - \Omega \tag{11}$$

$$b_0 = b - \Omega \tag{12}$$

$$h_0 = h + \Omega. \tag{13}$$

The formulation adds versatility to the model by considering the possibility that adjacent turns can be separated by a certain gap. The turn gap δ_{xy} shown in Fig. 4 is, therefore, defined. The distance between the centers of adjacent wires, denoted by D_{xy}, is related to the turn gap by means of Ω as

$$D_{xy} = \Omega + \delta_{xy}. \tag{14}$$

B. Self-Inductance of a Rectangular-Shaped Coil

The self-inductance L_{coil} of a rectangular coil with N turns can be calculated on only two of its four sides by taking advantage of the symmetrical geometry of the rectangle

$$L_{\text{coil}} = 2\left(L_{\text{side\_}a} + L_{\text{side\_}b}\right). \tag{15}$$

$L_{\text{side\_}a}$ and $L_{\text{side\_}b}$ represent the contribution of each of the sides with lengths a and b, respectively, to the total self-inductance of the coil. In turn, $L_{\text{side\_}a}$ is made up of three contributions that result from applying the superposition principle to any of the two coil sides of length a: the self-inductance of the N straight wires present on one of these sides (L_w), the mutual

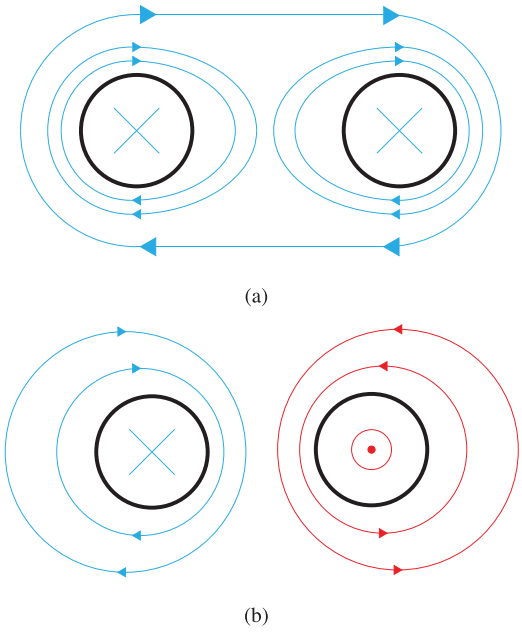

Fig. 5. Magnetic field lines around two equal and parallel straight conductors that lie on the same plane, when (a) the currents flow in the same direction and (b) the currents flow in opposite directions.

inductance among the N wires that lie on the same side (M_{ss}), and the mutual inductance among each of these N wires and the N wires that lie on the opposite side M_{os}. $L_{\text{side\_}b}$ results from applying the same principle to the two coil sides of length b. As the expressions for $L_{\text{side\_}a}$ and $L_{\text{side\_}b}$ share equivalent terms, they can be merged into a single common expression that is valid to calculate both

$$L_{\text{side}} = L_w + M_{ss} - M_{os}. \tag{16}$$

Note that no additional terms are necessary in (16), since the mutual inductance of perpendicular coil sides is negligible [15]. Furthermore, when the currents flow in the same direction (i.e., the wires belong to the same coil side), the magnetic fields around each wire add up, as shown in Fig. 5(a), and both the total magnetic field and the self-inductance L_{side} increase owing to the positive sign of M_{ss}. On the contrary, when the currents flow in opposite directions (in this case, the wires necessarily belong to opposite coil sides), the magnetic fields tend to compensate each other, as depicted in Fig. 5(b), causing a decrease in the total magnetic field and in the self-inductance L_{side} owing to the negative sign of M_{os}.

For the calculation of L_w, the coil was divided at its corners for convenience, as shown in Fig. 6. The total self-inductance of the N wires of any of the coil sides a and b results from adding up the following N individual contributions according to (1):

$$L_w = \sum_{i=0}^{N-1} L(l_i, \rho). \tag{17}$$

Taking the outer turn (numbered 0) as a reference, the length l_i of the straight ith wire on the sides of lengths a and b is,

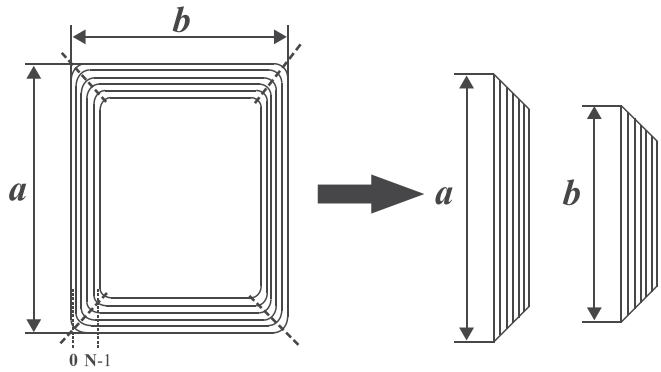

Fig. 6. Partitioning of a multiturn rectangular coil at its corners.

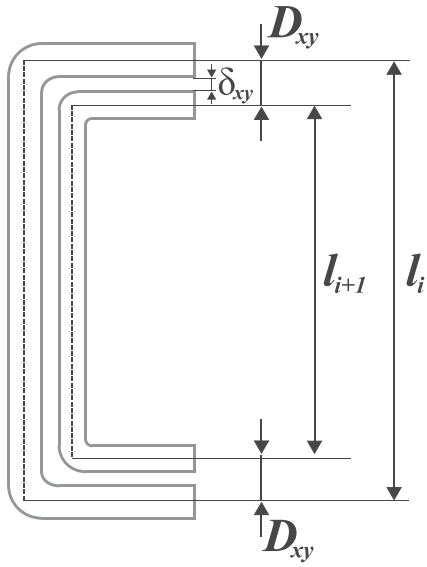

Fig. 7. Lengths l_i and l_{i+1} of two adjacent straight wires. Note that $l_{i+1} = l_i - 2D_{xy}$.

according to Fig. 7, given by

$$\begin{aligned} l_{i\_a} &= a_0 - 2iD_{xy} \\ l_{i\_b} &= b_0 - 2iD_{xy}. \end{aligned} \tag{18}$$

With regard to the derivations of M_{ss} and M_{os}, the use of (2), which is valid for wires of unequal lengths, was ruled out as it would add excessive complexity to the model. A tradeoff between accuracy and manageability was chosen by applying (10) instead. This approach prevents the model from becoming too intricate, without compromising accuracy to a great extent. A requirement that must be met prior to using (10) for the derivation of either M_{ss} or M_{os} is that all the wires involved in the calculation must be of equal length. This simplification, therefore, affects the calculations performed on only the corners of the coil. Two new averaged parameters, $\bar{a}$ and $\bar{b}$, were consequently defined as the corresponding side lengths of the wires located at the midpoints of the coil sides a and b. For illustration purposes, the averaged coil side $\bar{a}$ is depicted in Fig. 8. The averaged sides $\bar{a}$ and $\bar{b}$ obey the following expressions that can

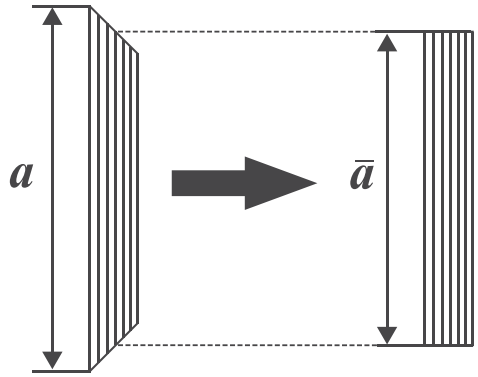

Fig. 8. Graphical definition of the average side length $\bar{a}$.

be deduced from an inspection of Figs. 7 and 8:

$$\bar{a} = a_0 - \frac{(N-1)}{2} \cdot 2D_{xy} = a_0 - (N-1)D_{xy}$$
$$\bar{b} = b_0 - \frac{(N-1)}{2} \cdot 2D_{xy} = b_0 - (N-1)D_{xy}. \quad (19)$$

Prior to determining each interaction among the N wires that lie on a given coil side, it is necessary to know the distance among their centers. The distance between any two of these N wires, termed as i and i', can be expressed as

$$d_{i-i'} = \begin{cases} (i-i')D_{xy}, & i > i' \\ (i'-i)D_{xy}, & i < i'. \end{cases} \quad (20)$$

M_{ss} is obtained for both side lengths by considering all the interactions among a given wire and the other $N-1$ wires that share the same coil side. The total number of contributions, therefore, amounts to $N \cdot (N-1)$

$$M_{ss\_a} = \sum_{i=0}^{N-1} \sum_{i'=0;i' \neq i}^{N-1} M(\bar{a}, d_{i-i'})$$
$$M_{ss\_b} = \sum_{i=0}^{N-1} \sum_{i'=0;i' \neq i}^{N-1} M(\bar{b}, d_{i-i'}). \quad (21)$$

The averaged side lengths $\bar{a}$ and $\bar{b}$ are again utilized in the derivation of M_{os}. Figs. 2 and 3 show the layout and the notation chosen to address the wires located on opposite sides of coil 1. For the sake of clarity, these two coil sides will henceforth be identified with the indexes that they carry, i and j. The distance between a straight wire located on side i and another wire on side j is, for a and b, respectively

$$d_{ij\_a} = a_0 - (i+j)D_{xy}$$
$$d_{ij\_b} = b_0 - (i+j)D_{xy}. \quad (22)$$

An expression for M_{os} that distinguishes between both side lengths follows upon the addition of the N^2 magnetic interactions existing among all the wires that lie on the sides i and j:

$$M_{os\_a} = \sum_{i=0}^{N-1} \sum_{j=0}^{N-1} M(\bar{a}, d_{ij\_a})$$
$$M_{os\_b} = \sum_{i=0}^{N-1} \sum_{j=0}^{N-1} M(\bar{b}, d_{ij\_b}). \quad (23)$$

Upon gathering together the previous derivations for L_w, M_{ss}, and M_{os}, (15) is expressed as follows:

$$L_{\text{coil}} = 2 \left[\sum_{i=0}^{N-1} \left(L(l_{i\_a}, \rho) + L(l_{i\_b}, \rho) \right) + \sum_{i=0}^{N-1} \sum_{i'=0;i' \neq i}^{N-1} \left(M(\bar{a}, d_{i-i'}) + M(\bar{b}, d_{i-i'}) \right) - \sum_{i=0}^{N-1} \sum_{j=0}^{N-1} \left(M(\bar{a}, d_{ij\_a}) + M(\bar{b}, d_{ij\_b}) \right) \right]. \quad (24)$$

C. Mutual Inductance for Two Single-Layer Rectangular Coils

The wire arrangement on which the derivation of the mutual inductance between coils 1 and 2 relies is depicted in Fig. 2. The notation based on the indexes utilized previously to unambiguously identify the opposite sides in the coil 1 will also be employed for coil 2.

Once again taking advantage of the symmetry, the derivation is reduced to the calculation of the mutual inductance of only two of the four sides of the rectangle, $M_{\text{side\_}a}$ and $M_{\text{side\_}b}$. The mutual inductance of the two coils can thus be written as

$$M_{\text{coil}} = 2\left(M_{\text{side\_}a} + M_{\text{side\_}b}\right). \quad (25)$$

In turn, $M_{\text{side\_}a}$ and $M_{\text{side\_}b}$ result from two contributions each, M_1 and M_2, which must be calculated separately for a and b

$$M_{\text{side}} = M_1 - M_2. \quad (26)$$

M_1 accounts for the mutual inductance between the side i of coil 1 and the corresponding side of coil 2 that lies closest to it (that is, the side k). In turn, M_2 expresses the mutual inductance between the side i of coil 1 and the side of coil 2 that lies furthest from it, which is t. Note that the signs in (26) depend on the direction of the currents. Assuming that the currents through the sides i and k flow in the same direction, it follows that M_1 has a positive sign. The currents through the sides i and t, therefore, have necessarily opposite directions, and M_2 is thus negative.

The derivation of M_1 and M_2 for a and b is shown in the following. The distance between the centers of two wires located on the sides i and k is common for both side lengths

$$d_{ik} = \sqrt{((i-k)D_{xy})^2 + h_0^2}. \quad (27)$$

When combining (10) and (27), M_1 is given by

$$M_{1\_a} = \sum_{i=0}^{N-1} \sum_{k=0}^{N-1} M(\bar{a}, d_{ik})$$
$$M_{1\_b} = \sum_{i=0}^{N-1} \sum_{k=0}^{N-1} M(\bar{b}, d_{ik}). \quad (28)$$

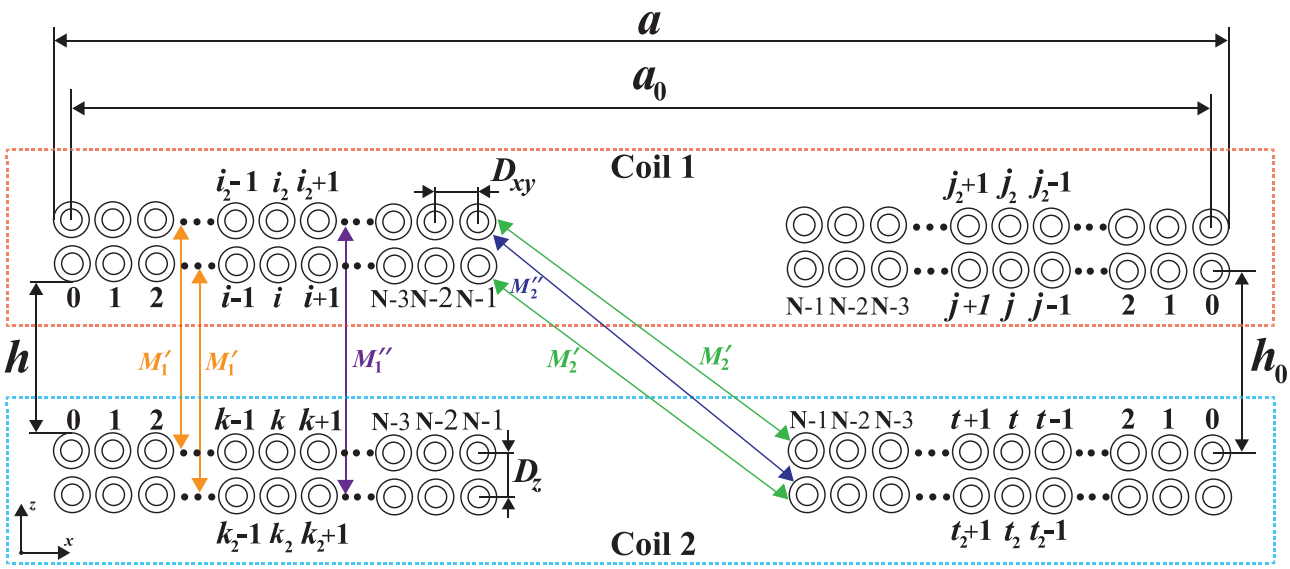

Fig. 9. Cross-sectional view of two equal, coaxial, and parallel double-layer coils with N turns per layer. The mutual inductance between two wires that belong to different coils is represented with the prime and the double prime symbol in order to distinguish those wires that are closest to and furthest from each other, respectively.

The distance between the centers of two wires located on the opposite sides i and t is calculated with different expressions for a and b as

$$d_{it\_a} = \sqrt{(b_0 - (i+t)D_{xy})^2 + h_0^2}$$
$$d_{it\_b} = \sqrt{(a_0 - (i+t)D_{xy})^2 + h_0^2}. \tag{29}$$

Upon combining (10) and (29), M_2 is given by

$$M_{2\_a} = \sum_{i=0}^{N-1}\sum_{t=0}^{N-1} M(\bar{a}, d_{it\_a})$$
$$M_{2\_b} = \sum_{i=0}^{N-1}\sum_{t=0}^{N-1} M(\bar{b}, d_{it\_b}). \tag{30}$$

When gathering together the previous derivations of M_1 and M_2, (25) is expressed as follows:

$$M_{\text{coil}} = 2\left[\sum_{i=0}^{N-1}\sum_{k=0}^{N-1}\left(M(\bar{a}, d_{ik}) + M(\bar{b}, d_{ik})\right) - \sum_{i=0}^{N-1}\sum_{t=0}^{N-1}\left(M(\bar{a}, d_{it\_a}) + M(\bar{b}, d_{it\_b})\right)\right]. \tag{31}$$

The previous derivation is valid for coils with an equal number of turns. For the more general case of coil couplers with a nonunity turns ratio, the additional interactions corresponding to the extra turns could be easily evaluated by following the outlined derivation.

Note that the conditions under which (10) strictly applies limit the scope of the previous derivation to the case of perfectly aligned coils. If a noticeable misalignment occurs, the model equation (31) will fail to yield reliable figures for the mutual inductance. In this case, the model must be built from the more general equation (9).

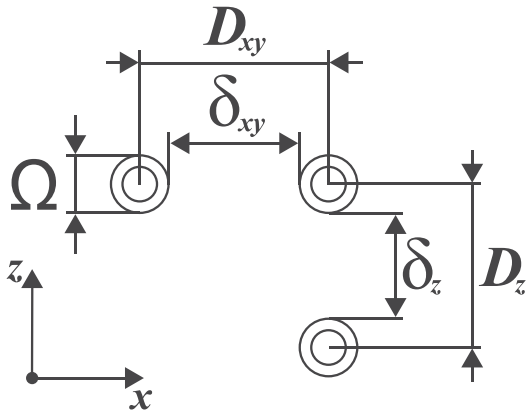

Fig. 10. Definition of the turn gap δ_z and the distance D_z between adjacent wires along the z-axis.

IV. Modeling of Two Double-Layer Coupled Coils

The self-inductance and mutual inductance derivations carried out for single-layer coils can be extended to coils with multiple layers. For coils with p layers, the total number of interactions among layers that must be taken into account in the calculation increases rapidly with p, amounting to $2p-1$ for the self-inductance and to $2p^2$ for the mutual inductance. The case for equal coils featuring a top layer and a bottom layer, both with N turns, is solved in this section. The formulation is based on the coil arrangement depicted in Fig. 9.

The second layer present in the coil arrangement requires that both the turn gap and the distance between wires defined in Fig. 4 along the x and y coordinates for the single layer case also be considered along the z-axis. Fig. 10 represents the corresponding

parameters, where

$$D_z = \Omega + \delta_z. \tag{32}$$

A. Self-Inductance of a Double-Layer Rectangular Coil

The derivation employed to obtain the self-inductance of a rectangular coil with two equal layers, one of which is piled up on top of the other, begins by adding two new terms to (16). One of them, M'_{ss}, accounts for the mutual inductance of the N wires that lie on the bottom layer of the side i and the N wires that are on the top layer of the same side (which is the added layer). The second term, M'_{os}, represents the mutual inductance of the N wires that lie on the bottom layer of the side i and the N wires located on the top layer of the opposite side, j. The signs of the added terms are consistent with the direction of the current flowing through the coil. Moreover, since the two layers in the coil are identical, the calculation is reduced in order to compute the interactions among one of the sides in a layer and the other three sides. Upon adding up the two new contributions, L_{side} is expressed as

$$L_{\text{side}} = 2\left(L_w + M_{ss} + M'_{ss} - M_{os} - M'_{os}\right) \tag{33}$$

where the symmetry of the double-layer structure justifies the factor 2.

The derivation of M'_{ss} and M'_{os} is shown in the following. The distance between a wire on the bottom layer of the side i and another wire on the top layer of the same side obeys an expression that is general for a and b

$$d_{i-i_2} = \sqrt{((i-i_2)D_{xy})^2 + D_z^2}. \tag{34}$$

When combining (10) and (34), the splitting of M'_{ss} into the corresponding equations for a and b results in

$$\begin{aligned} M'_{ss\_a} &= \sum_{i=0}^{N-1}\sum_{i_2=0}^{N-1} M(\bar{a}, d_{i-i_2}) \\ M'_{ss\_b} &= \sum_{i=0}^{N-1}\sum_{i_2=0}^{N-1} M(\bar{b}, d_{i-i_2}). \end{aligned} \tag{35}$$

Furthermore, the distances between a wire on the bottom layer of the side i and another wire on the top layer on the opposite side are

$$\begin{aligned} d_{i-j_2\_a} &= \sqrt{(b_0 - (i+j_2)D_{xy})^2 + D_z^2} \\ d_{i-j_2\_b} &= \sqrt{(a_0 - (i+j_2)D_{xy})^2 + D_z^2}. \end{aligned} \tag{36}$$

Upon combining (10) and (36), M'_{os} is written as

$$\begin{aligned} M'_{os\_a} &= \sum_{i=0}^{N-1}\sum_{j_2=0}^{N-1} M\left(\bar{a}, d_{i-j_2\_a}\right) \\ M'_{os\_b} &= \sum_{i=0}^{N-1}\sum_{j_2=0}^{N-1} M(\bar{b}, d_{i-j_2\_b}). \end{aligned} \tag{37}$$

B. Mutual Inductance of Two Double-Layer Rectangular Coils

The initial expression employed to derive the mutual inductance for the double-layer magnetic coupler is (26). If the extra terms corresponding to the interactions M'_1, M''_1, M'_2, and M''_2, which are necessary to account for the influence of the new layer and are represented by arrows in Fig. 9, are added to (26), M_{side} is calculated for any of the sides a and b using

$$M_{\text{side}} = M_1 + 2M'_1 + M''_1 - M_2 - 2M'_2 - M''_2. \tag{38}$$

The distances involved in the derivations of M'_1 and M'_2 for a and b are obtained by adding D_z to (27) and (29), as follows:

$$d'_{ik} = \sqrt{((i-k)D_{xy})^2 + (h_0 + D_z)^2} \tag{39}$$

$$\begin{aligned} d_{it\_a} &= \sqrt{(b_0 - (i+t)D_{xy})^2 + (h_0 + D_z)^2} \\ d_{it\_b} &= \sqrt{(a_0 - (i+t)D_{xy})^2 + (h_0 + D_z)^2}. \end{aligned} \tag{40}$$

Upon combining (39) and (40) with (10), M'_1 and M'_2 are written as

$$\begin{aligned} M'_{1\_a} &= \sum_{i=0}^{N-1}\sum_{k=0}^{N-1} M(\bar{a}, d'_{ik}) \\ M'_{1\_b} &= \sum_{i=0}^{N-1}\sum_{k=0}^{N-1} M(\bar{b}, d'_{ik}) \end{aligned} \tag{41}$$

$$\begin{aligned} M'_{2\_a} &= \sum_{i=0}^{N-1}\sum_{t=0}^{N-1} M(\bar{a}, d'_{it\_a}) \\ M'_{2\_b} &= \sum_{i=0}^{N-1}\sum_{t=0}^{N-1} M(\bar{b}, d'_{it\_b}). \end{aligned} \tag{42}$$

In the case of the mutual inductances M''_1 and M''_2, the corresponding distances are affected by the factor $2D_z$

$$d''_{ik} = \sqrt{((i-k)D_{xy})^2 + (h_0 + 2D_z)^2} \tag{43}$$

$$\begin{aligned} d''_{it\_a} &= \sqrt{(b_0 - (i+t)D_{xy})^2 + (h_0 + 2D_z)^2} \\ d''_{it\_b} &= \sqrt{(a_0 - (i+t)D_{xy})^2 + (h_0 + 2D_z)^2}. \end{aligned} \tag{44}$$

When combining (43) and (44) with (10), M''_1 and M''_2 are written as

$$\begin{aligned} M''_{1\_a} &= \sum_{i=0}^{N-1}\sum_{k=0}^{N-1} M(\bar{a}, d''_{ik\_a}) \\ M''_{1\_b} &= \sum_{i=0}^{N-1}\sum_{k=0}^{N-1} M(\bar{b}, d''_{ik\_b}) \end{aligned} \tag{45}$$

$$\begin{aligned} M''_{2\_a} &= \sum_{i=0}^{N-1}\sum_{t=0}^{N-1} M(\bar{a}, d''_{it\_a}) \\ M''_{2\_b} &= \sum_{i=0}^{N-1}\sum_{t=0}^{N-1} M(\bar{b}, d''_{it\_b}). \end{aligned} \tag{46}$$

V. Case of In-Plane Misalignment

A lateral offset between the two coils of the magnetic coupler is to be expected, depending on the application. This is the case of contactless EV charging, in which some sensing systems have been reported to aid the vehicle alignment, as in [27]. The previous formulation is suitable for EV applications, provided

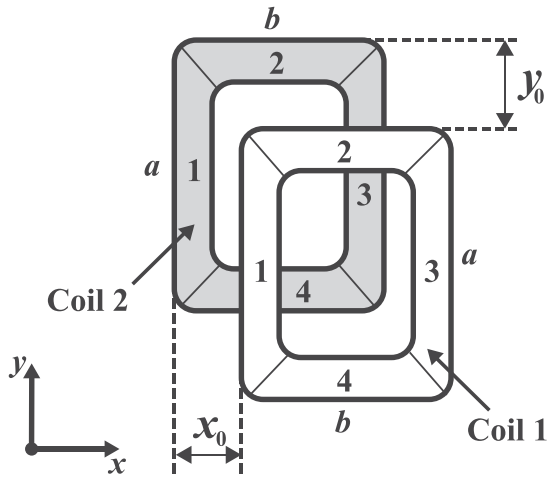

Fig. 11. Layout of a rectangular magnetic coupler with misaligned coils, showing the numbering of the coil sides and the lateral offsets x_0 and y_0.

that the charging station is equipped with an alignment sensing system. However, if such a system is not available, it is desirable to extend the proposed formulation and cover a more realistic charging scenario in which lateral misalignment on the xy plane occurs.

For the sake of brevity, the modeling of misalignment applies to single-layer coils only. The in-plane misalignment is taken into account by using (9) rather than (10). According to the layout of the magnetic coupler depicted in Fig. 11, in which lateral offsets x_0 and y_0 are introduced, the parameter Δ that was defined in Fig. 1 for a unidimensional case can be expressed as follows, in order to distinguish between the a and b coil sides:

$$\begin{aligned}\Delta_a &= -(a - y_0) = y_0 - a\\ \Delta_b &= -(b - x_0) = x_0 - b.\end{aligned} \tag{47}$$

Unlike in the previous sections, in which it was possible to simplify derivations owing to the symmetry of the rectangle, the presence of an in-plane lateral offset between the coils obliges us to consider the magnetic interactions on all four sides of the rectangle no two by two, but individually. M_{coil} is, therefore, expressed as follows:

$$M_{\text{coil}} = M_1 - M_2 = \sum_{n=1}^{4} M_{1,n} - \sum_{n=1}^{4} M_{2,n} \tag{48}$$

where the index n runs from 1 to 4 and refers to each of the rectangle sides, as shown in Fig. 11. The distances among wires must be recalculated to account for x_0 and y_0. With regard to M_1, the calculation can be simplified by considering that only two distances are required, since $M_{1,1} = M_{1,3}$ and $M_{1,2} = M_{1,4}$

$$\begin{aligned}d_{ik\_1} &= \sqrt{((i-k)D_{xy} + x_0)^2 + h_0^2}\\ d_{ik\_2} &= \sqrt{((i-k)D_{xy} + y_0)^2 + h_0^2}.\end{aligned} \tag{49}$$

Combining (9) and (49), M_1 is written as

$$M_1 = 2\sum_{i=0}^{N-1}\sum_{k=0}^{N-1}\Big(M_\Delta(\bar{a}, d_{ik\_1}, \Delta_a) + M_\Delta(\bar{b}, d_{ik\_2}, \Delta_b)\Big). \tag{50}$$

However, all four $M_{2,k}$ are different, and the calculation for M_2, therefore, involves the four following distances, as follows from an inspection of Fig. 10:

$$\begin{aligned}d_{it\_1} &= \sqrt{(b_0 - (i+t)D_{xy} - x_0)^2 + h_0^2}\\ d_{it\_2} &= \sqrt{(a_0 - (i+t)D_{xy} - y_0)^2 + h_0^2}\\ d_{it\_3} &= \sqrt{(b_0 - (i+t)D_{xy} + x_0)^2 + h_0^2}\\ d_{it\_4} &= \sqrt{(a_0 - (i+t)D_{xy} + y_0)^2 + h_0^2}.\end{aligned} \tag{51}$$

Upon combining (9) and (51), M_2 is written as

$$\begin{aligned}M_2 = \sum_{i=0}^{N-1}\sum_{t=0}^{N-1}\Big(&M_\Delta(\bar{a}, d_{it\_1}, \Delta_a) + M_\Delta(\bar{b}, d_{it\_2}, \Delta_b)\\ &+ M_\Delta(\bar{a}, d_{it\_3}, \Delta_a) + M_\Delta(\bar{b}, d_{it\_4}, \Delta_b)\Big).\end{aligned} \tag{52}$$

Fig. 12 shows a flowchart in which the decision tree used by the model in the inductance calculations is illustrated.

VI. Inductance Calculations Based on the Reduction to a Single-Turn Coil

The double-layer coils modeled with the formulation derived previously can alternatively be modeled using a different method. This second approach relies on expressions that were not purposely deduced for an actual coil with its own geometrical features, as is the case of the proposed model, but for an ideal circuit instead. Keeping in mind that the proposed model will be experimentally validated using square-shaped coils, the alternative formulation that follows applies to a square geometry.

Although the calculations involved are relatively straightforward, we shall show that the accuracy obtained is, to some extent, compromised. The underlying idea that allows us to apply this alternative formulation to actual square coils relies on the reduction of an actual coil to an imaginary single-turn coil that can be regarded as an equivalent square turn whose radius and side length are determined from geometrical features of the original coil. In order to illustrate the reduction process, Fig. 13(a) shows the transformation of a double-layer coil with three turns per layer and an outer side length a into an imaginary equivalent coil formed of a single turn with a finite wire radius ρ_{eq} and an average side $\bar{a}$, where $\bar{a}$ is the distance between the centers of opposite coil sides. Furthermore, the distance between the two mutually coupled coils, d, is taken at their middle points, as depicted in Fig. 13(b). The equivalent radius ρ_{eq} of the imaginary coil is calculated by assuming that the resulting cross-sectional area matches the total area of the six original turns [see Fig. 13(c)].

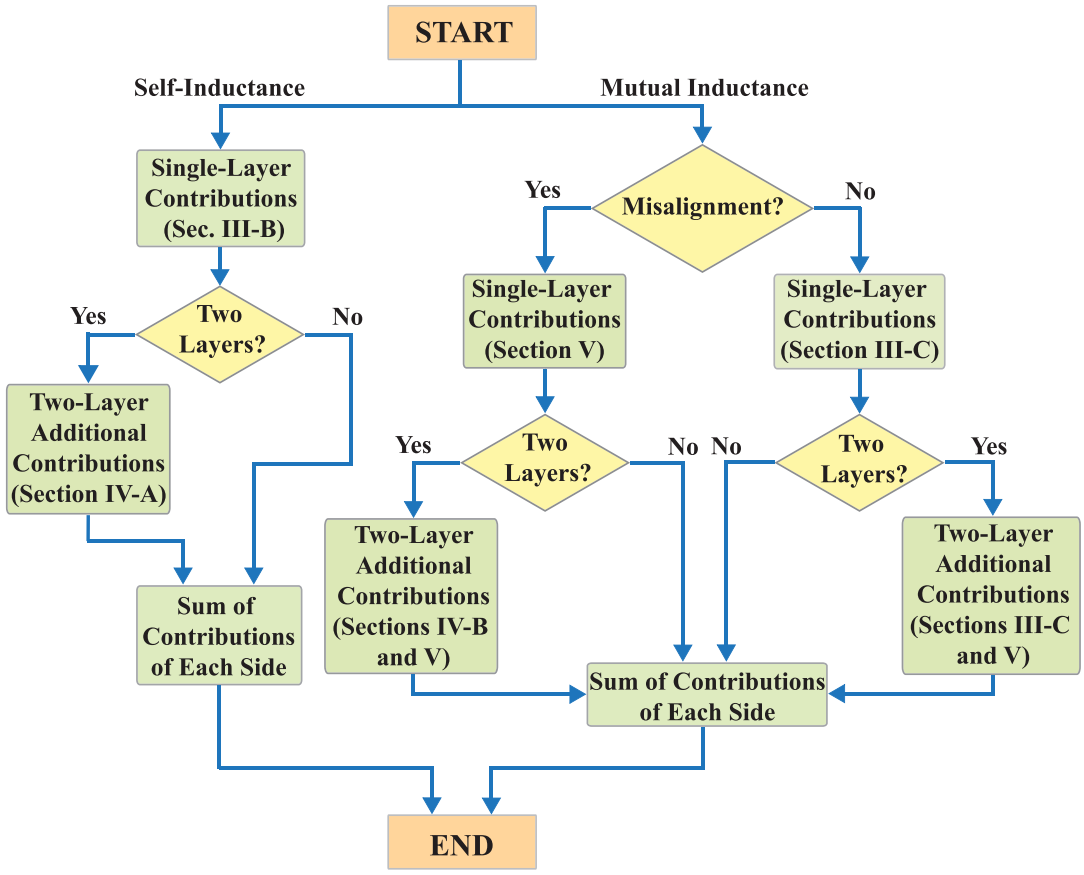

Fig. 12. Flowchart with the decision tree followed by the proposed model.

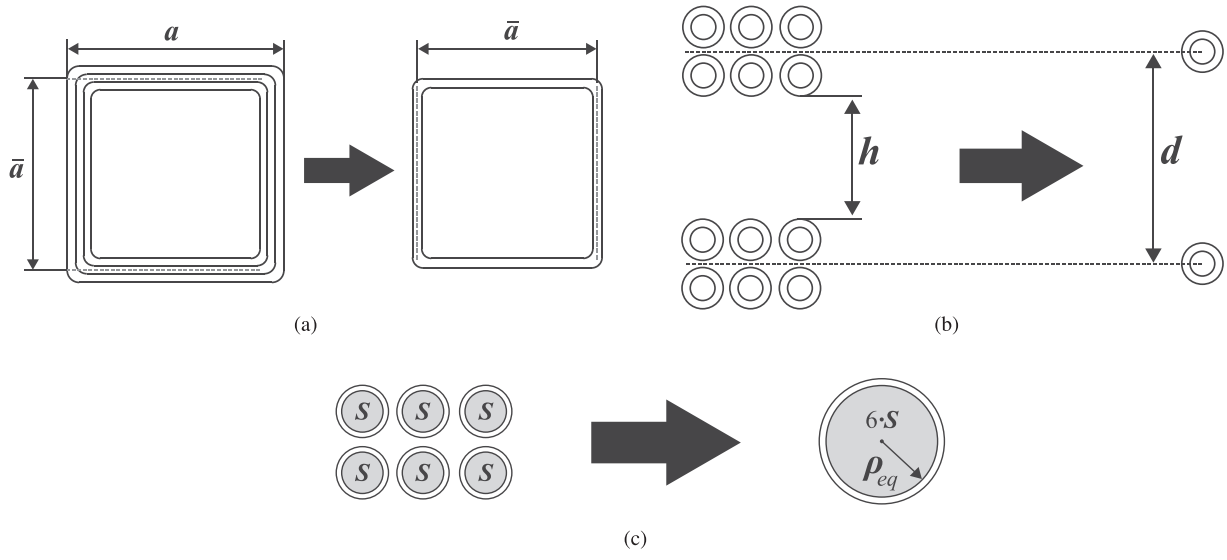

Fig. 13. Reduction process of a double-layer coil with three turns per layer to an equivalent single-turn coil. (a) Definition of the average side $\bar{a}$ of the single turn coil. (b) Distance b between the centers of the two double-layer coils. (c) Definition of the equivalent radius ρ_{eq}.

For an actual double-layer coil with $2N$ turns and a cross-sectional area per turn S, the equivalent turn radius of the imaginary coil is

$$\rho_{\text{eq}} = \sqrt{\frac{2NS}{\pi}}. \tag{53}$$

Upon using the previously defined parameters, the expression for the self-inductance L_{eq} of the imaginary coil, which is assumed to be equivalent to the double-layer square coil under consideration, can be readily adapted from [23] and is given by the following expression:

$$L_{\text{eq}} = \frac{\mu_0}{4\pi}(2N)^2 8\bar{a}\left(\ln\left(\frac{\bar{a}}{\rho_{\text{eq}}}\right) - 0.77401 + \frac{\mu}{4}\right) \tag{54}$$

where μ is the permeability of the wire material. For the usual case of nonmagnetic materials, $\mu = 1$. The equivalent mutual inductance of the two imaginary coils, M_{eq}, can be expressed as [17]

$$M_{\text{eq}} = \frac{\mu_0}{4\pi}(2N)^2 8\left[\bar{a}\ln\left(\frac{\sqrt{d^2+\bar{a}^2}+d^2+\bar{a}^2}{d\cdot\bar{a}+d\cdot\sqrt{d^2+2\bar{a}^2}}\right) + \sqrt{2\bar{a}^2+d^2} - 2\sqrt{\bar{a}^2+d^2} + d\right]. \tag{55}$$

Although this simplified approach is not expected to provide an outstanding accuracy, it was tested with acceptable results for the case of M_{eq} and a separation between two double-layer square coils of 125 and 150 mm [28], [29]. Both air gaps are of practical interest in IPT systems for light-duty EVs.

VII. Setup of the FEA Models

A set of simulation models was set up in order to test the behavior of the analytical model in a wide range of situations without the need of winding additional coils with different features. The piece of software selected for the three-dimensional (3-D) electromagnetic modeling of the magnetic coupler is EMS (by EMWORKS), which works as a plug-in for Solidworks. For the whole set of simulation models presented in this article, an iterative solver based on the Newton–Raphson numerical method was used. In order to achieve a good matching between experimental and simulation results, a relative residual error of 1×10^{-6} was set up for every simulation run. This means that a given simulation will continue until the deviation between two consecutive iterations falls below that error.

Fig. 14 shows the magnetic coupler in the Solidworks environment. There are two concentric spheres around the coupler in order to model the surrounding medium of the coils, which is air. The outer sphere defines the boundaries of the model, whereas the inner sphere is necessary to reach the required accuracy in the field distribution around the coils. For the case of long coil sides (up to 500 mm), an iterative process results in diameters of 1250 and 2500 mm for the inner and outer spheres, respectively. For small coil sides (up to 50 mm), the corresponding diameters are 150 and 300 mm. Once the model geometry is defined, a 3-D mesh formed by tetrahedral elements was built in order to generate the nodes for the solver. In a further step, the optimal

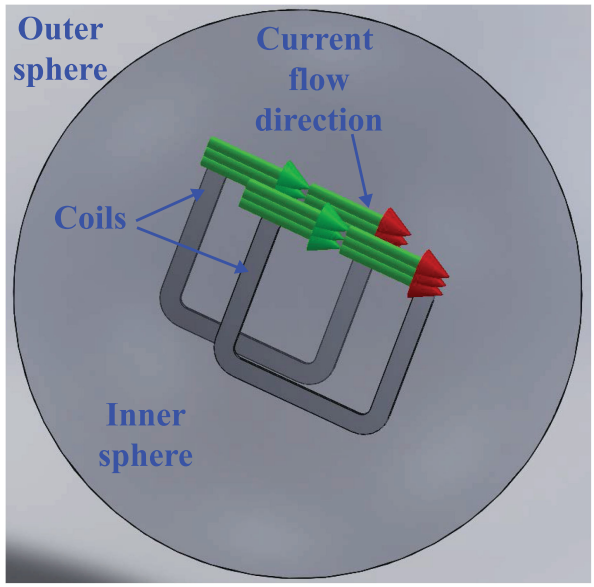

Fig. 14. Air-core magnetic coupler in EMS.

TABLE I
Maximum Mesh Size (in Millimeters) of the Different Elements in the FEA Model

Element	Big coils	Small coils
Coils	5	0.25
Inner sphere	15	2
Outer sphere	Automatically defined by EMS	

mesh size of every element in the model, shown in Table I, was determined after a convergence process. As can be seen, while the maximum mesh size of the inner sphere is a parameter of the user settings, the corresponding mesh size of the outer sphere can optionally be set automatically by the software to a value greater than that of the inner sphere, considering that the field intensity decays considerably with the distance to the coils.

Coils are modeled as a solid that has the same section as the entire coil side. By using the *wound coil* option of EMS, a coil with a given number of turns that is wound with a wire of a certain diameter can be simulated. After entering these settings, the software distributes the total wire section over the cross section of the solid coil and set the remaining surface as a dielectric nonmagnetic material. The arrows shown in Fig. 14 show the direction of the current flow in each coil.

VIII. Experimental Validation

The degrees of accuracy attained with the proposed model, the alternative model (which will henceforth be referred to as the single-turn model), and the simulation model were evaluated using experimental measurements carried out on two air-core magnetic couplers constructed with different dimensions for comparison and validation purposes. One of them features two double-layered coaxial square coils with 11 turns per layer, whose turns were wound using Litz wire formed by 800 strands of 0.1 mm of diameter with a circular cross-sectional area of

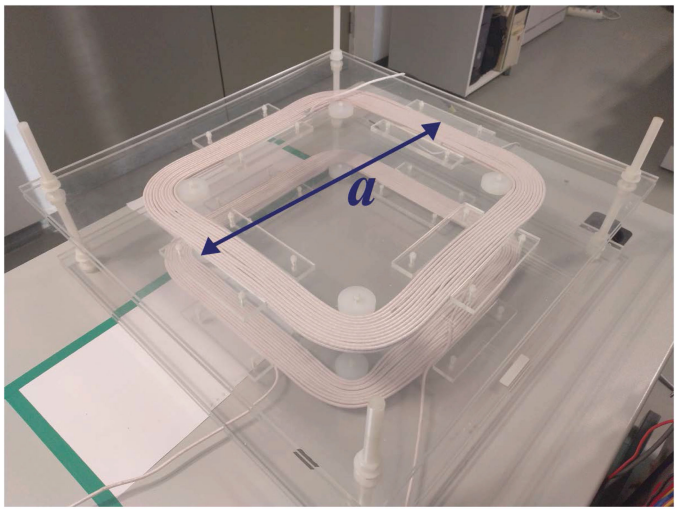

(a)

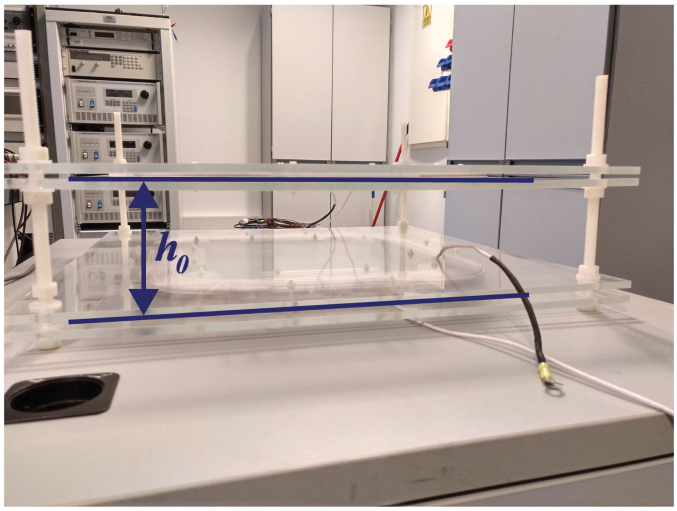

(b)

Fig. 15. Two views of one of the magnetic couplers, featuring double-layered square coils, utilized for the validation of the proposed model. (a) Top view. (b) Side view.

6.28 mm^2. This magnetic coupler, which is shown in Fig. 15 for illustration purposes, is the core of a 2-kW IPT prototype with a switching frequency of 18.65 kHz designed for the wireless charging of EVs whose performance and modeling can be found in [30] and [31], respectively. The second magnetic coupler is smaller and features two single-layered coaxial rectangular coils with ten turns per layer, using Litz wire formed by 400 strands of 0.1 mm of diameter and a circular cross-sectional area of 3.14 mm^2. Though the frequency of operation of a given IPT system varies with the application, the nominal switching frequency, f, is 85 kHz in the case of wireless charging of light-duty EVs according to the SAE-J2954 standard. Taking this frequency as a reference value and using (56) to determine the skin depth δ [32], where σ is the metal conductivity, the value obtained for δ in the conductor is 0.226 mm, which is above the strand diameter of the Litz wire used in any of the two coil designs. Therefore, both the skin effect and the current displacement are negligible, and a uniform current distribution can safely be assumed in both cases

$$\delta = \frac{1}{\sqrt{\pi f \mu_0 \sigma}}. \tag{56}$$

The self-inductances of the primary and secondary coils, L_1 and L_2, were measured with an Agilent 4294 A precision impedance analyzer. For validation purposes, the coupling coefficient k was obtained experimentally for seven air gaps between coils in the range of 50–200 mm, taken at 50-mm intervals. For each air gap, k was calculated from four voltage measurements carried out on the inductive coupler following the voltage ratio method described in [33]. In this method, one of the coils is fed with a sinusoidal voltage, and the induced voltage across the other coil is measured. In a second step, the coils are swapped before repeating the voltage measurement. The coupling coefficient can be readily obtained once the ratios between the induced and the applied voltages are calculated in both cases. For accuracy reasons, it is convenient to select a driving voltage with a high amplitude and frequency. The peak-to-peak amplitude for each voltage signal was averaged 1000 times in order to filter out electrical noise. Further details of this method when applied to an initial prototype of the square magnetic coupler under study for the three air gaps of 125, 150, and 175 mm can be found in [31]. Once L_1, L_2, and k are known, M can be calculated using the following expression:

$$M = k\sqrt{L_1 L_2}. \tag{57}$$

The experimental values of L_1, L_2, k, and M are shown in Table II, in which M and k were obtained for the air gap of 125 mm. This intermediate gap was chosen in order to provide the parameters entered in the models that follow below, along with a comparison of the numerical results obtained with them.

TABLE II
EXPERIMENTAL CHARACTERIZATION OF THE TWO MAGNETIC COUPLERS UNDER TEST

	Coil geometry	
Parameter	*Square*	*Rectangular*
L_1 (μH)	395	54
L_2 (μH)	389	57
M (μH)	89.29	7.88
k	0.2278	0.1427

M and k correspond to an air gap of 125 mm.

A. Accuracy of the Proposed Model

As the primary and secondary coils of each magnetic coupler were wound manually, their corresponding dimensions do not exactly match (though they are quite similar). Some of the geometrical parameters utilized to validate the proposed model consequently correspond to averaged values measured on the four sides of the coils. Table III shows the set of parameters that are common to both coils for each magnetic coupler, whereas Tables IV and V contain the averaged values that are slightly different for each coil. While Ω is an experimental measurement,

TABLE III
COMMON PARAMETERS TO BOTH COILS OF EACH MAGNETIC COUPLER, FOR VALIDATION PURPOSES

	Coil geometry	
Parameter	*Square*	*Rectangular*
h (mm)	125	125
ρ (mm)	1.415	1.000
Ω (mm)	3.80	2.70
δ_z	0	0
N	11	10

TABLE IV
PARAMETERS THAT DIFFER BETWEEN THE COILS OF THE SQUARE MAGNETIC COUPLER, FOR VALIDATION PURPOSES

Parameter	**Coil 1**	**Coil 2**	**Average**
a (mm)	42.55	42.45	42.50
δ_{xy} (mm)	0.270	0.395	0.330

TABLE V
PARAMETERS THAT DIFFER BETWEEN THE COILS OF THE RECTANGULAR MAGNETIC COUPLER, FOR VALIDATION PURPOSES

Parameter	**Coil 1**	**Coil 2**	**Average**
a (mm)	32.2	32.4	32.3
b (mm)	25.4	25.5	25.45
δ_{xy} (mm)	0.58	0.55	0.565

TABLE VI
CHARACTERIZATION OF THE TWO MAGNETIC COUPLERS UNDER TEST PROVIDED BY THE PROPOSED MODEL FOR AN AIR GAP OF 125 mm, INCLUDING DEVIATIONS FROM THE EXPERIMENT

	Square coils		**Rectangular coils**	
Parameter	*Value*	ε_r (%)	*Value*	ε_r (%)
L_1 (μH)	408.34	3.38	57.24	6.00
L_2 (μH)	401.50	3.21	57.94	1.65
M (μH)	90.86	1.76	7.99	1.38
k	0.2318	1.76	0.1447	1.38

ρ was deduced from the cross-sectional area of the Litz wire provided by the manufacturer.

The values for L_1, L_2, k, and M that result from applying the proposed model with the geometrical parameters shown in Tables III–V are grouped in Table VI, along with the relative errors ε_r that were calculated taking the experimental measurements shown in Table II as a reference. Note that the value of k results from combining the analytical value of M provided by the model with the experimental measurements of L_1 and L_2, and it is for this reason that the corresponding relative errors are equal.

As can be seen in Table VI, the deviations that appear between the values provided by the model and by the experiment are remarkably low in all cases. Note that the model behaves slightly better as regards determining the mutual inductance than in the case of any of the two self-inductances. The ability of the model to, on the one hand, take into account every interaction among all the turns and to, on the other, include the tiny separation between adjacent turns that inevitably arise owing to the manual winding of the wire justifies the good agreement found between the experimental and the analytical results.

TABLE VII
PARAMETER SET USED TO TEST THE SINGLE-TURN MODEL

Parameter	**Value**
$\bar{a}$ - Coil 1 (cm)	38.05
$\bar{a}$ - Coil 2 (cm)	38.27
Averaged $\bar{a}$ (cm)	38.16
d (mm)	132.6
S (mm^2)	6.28

B. Accuracy of the Single-Turn and FEA Models, and Comparison With the Proposed Model

Table VII shows the parameters entered in the single-turn model. The FEA modeling was carried out with the values shown in Tables III–V. The inductance values obtained with these sets of parameters and the corresponding relative errors that result upon comparison with the experiments are shown in Table VIII.

It is apparent that the single-turn model is not suitable to calculate the self-inductances L_1 and L_2 correctly, since it fails to yield reliable values (the relative errors are above 30% in both cases). These large-error figures result from the limitations inherent to (54) when this expression is utilized to model an actual coil, as it was derived for an ideal closed circuit. The numerous interactions among all the turns in an actual coil are not evaluated individually with (54); instead, the added factor $(2N)^2$ is a rough attempt to account for the multiplicity of turns present in the actual arrangement. Moreover, the separation between adjacent turns is not considered in the model, which adds up to the sources of error.

With regard to M, the deviation from the experimental value is remarkably lower than in the case of the self-inductances. This can be explained by taking into account that not every geometrical coil feature exerts the same influence on the coupling coefficient k [34]–[36]: while neither the separation between adjacent turns nor the radius of the wound wire have a major influence on k, both the inner and the outer side lengths of the coils, which determine the coil width, *do* greatly influence k. It was, therefore, convenient to define the side length $\bar{a}$ of the equivalent single-turn coil as the length of the middle turn in the actual coils, since it can be regarded as an averaged value between the outer and the inner turn lengths. Note, however, that the agreement with the experimental value, while acceptable, is not as good as that attained with the proposed model.

Fig. 16(a) extends the previous validation study by representing, on the same plot, the calculated coupling coefficient k obtained with the three models and their experimental counterparts for the seven measurements available, restricted to the coils with square geometry. Upon inspecting the plot, it follows that, although the deviation found with either of the three models with respect to the experimental data are small, especially for larger air gaps, the proposed model performs noticeably better

TABLE VIII
CHARACTERIZATION OF THE TWO MAGNETIC COUPLERS UNDER TEST PROVIDED BY THE FEA AND SINGLE-TURN MODELS FOR AN AIR GAP OF 125 mm, INCLUDING DEVIATIONS FROM THE EXPERIMENT

	Square coils				**Rectangular coils**	
	Single-turn model		*FEA model*		*FEA model*	
Parameter	*Value*	ε_r (%)	*Value*	ε_r (%)	*Value*	ε_r (%)
L_1 (μH)	519.43	31.50	397.50	0.63	54.65	1.96
L_2 (μH)	523.38	34.54	390.70	0.39	55.12	3.03
M (μH)	92.19	3.25	88.06	1.38	7.68	2.45
k	0.2352	3.25	0.2246	1.38	0.1392	2.45

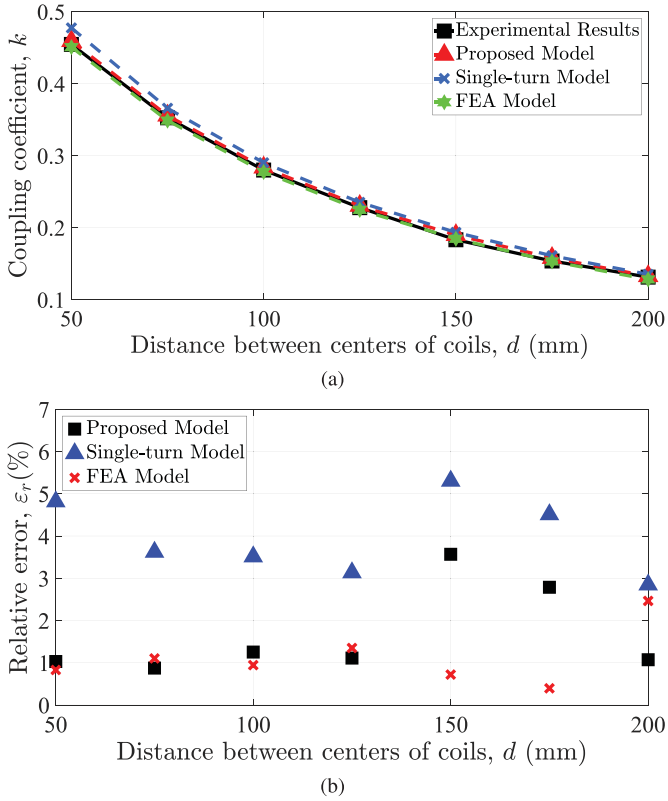

Fig. 16. Coupling coefficient k for several air gaps between coils in the case of the square magnetic coupler. (a) Comparison between experimental and predicted results. (b) Relative errors that result from predictions of the different models.

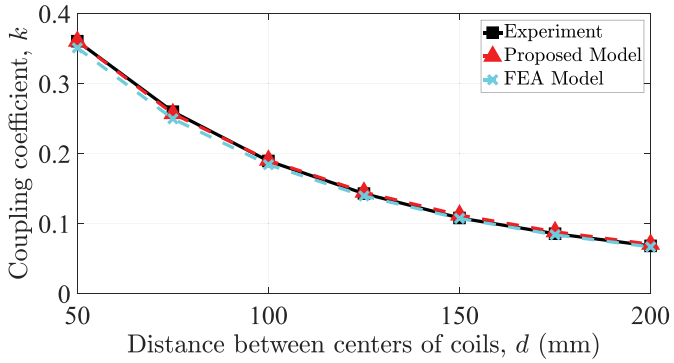

Fig. 17. Coupling coefficient k for several air gaps between coils in the case of the rectangular magnetic coupler. Comparison between experimental and predicted results.

than the single-turn model in all cases. The same conclusion is reached when representing the relative errors with respect to the experiment, which are always below 4% for the proposed model, as Fig. 16(b) shows. As can be seen in Fig. 17, the behavior of the proposed and the FEA models is also satisfactory when applied to the rectangular coils. In this case, the relative errors are always below 5%. This allows us to assess the validity of the proposed model for accurate inductance calculations on both rectangular and square geometries. It should be pointed out that the small deviations from the experiment found with the FEA model demonstrate its reliability to be used with some other cases described in Section IX that cannot be verified experimentally.

C. Accuracy of the Proposed Model With In-Plane Misalignment

A total of five sets of experimental measurements were carried out to determine the influence on the coupling coefficient k of a lateral offset of one coil with respect to the other in one and two dimensions for the square and the rectangular coils. Both cases will be analyzed separately in the following.

Fig. 18 shows the setup for the case of an in-plane misalignment between the square coils along the x and y axes depicted in Fig. 11.

A first set of 12 measurements was taken for a 1-D lateral offset x_0 along the x-axis, which ranged from 0 to 300 mm. A second set was measured for a series of equal lateral offsets x_0 and y_0 along the x and y axes simultaneously. This gave rise to 12 (x_0, y_0) displacements following the diagonal line common to both coils, starting in (0, 0) and ending in (300, 300) mm, which represents a 70% of the outer side length of the coils. In all cases, the air gap h was set to 123 mm.

The experimental results and their theoretical and FEA counterparts are represented in Fig. 19(a). As can be seen, the models satisfactorily predict the decreasing trend of k found as the misalignment increases for both cases. This nonlinear decreasing trend coincides with that shown in other works [36]–[38]. It should be noted that for sufficiently large 2-D misalignments (around 300 mm), the coupling coefficient k is negative. An experimentally detected phase shift of 180° between the voltage signals on the primary and secondary sides is in agreement

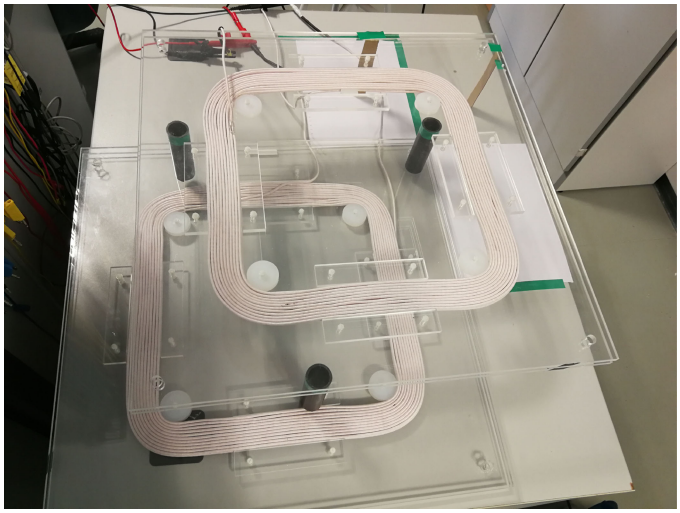

Fig. 18. Setup employed to perform in-plane misalignment measurements on the square coils.

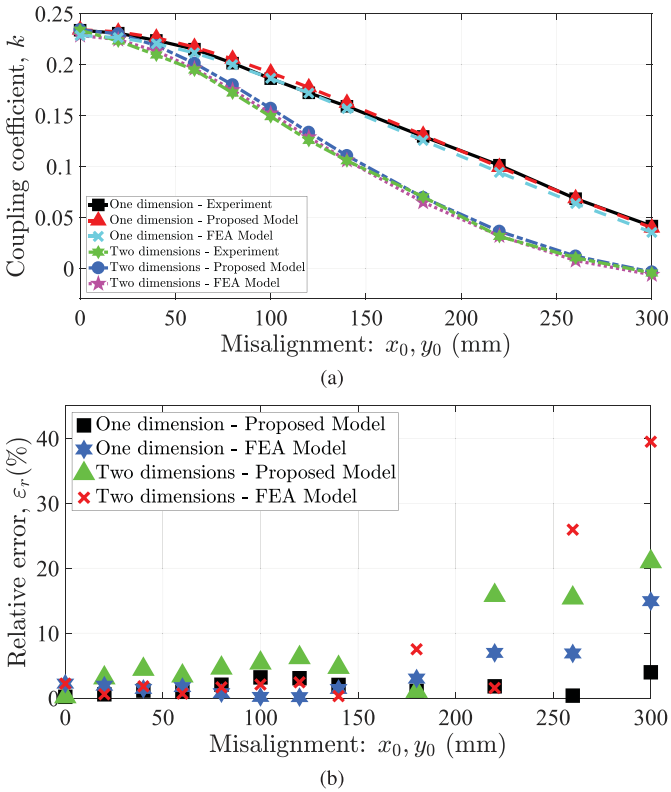

Fig. 19. Coupling coefficient k for lateral offsets in one and two dimensions for square coils. (a) Comparison with experimental results. (b) Relative errors.

with the change of sign. This effect was previously observed in [18] and [39]. Moreover, it is apparent from an inspection of Fig. 19(b), which shows the relative errors, that they are reasonably low except when the coupling coefficient is very small ($k < 0.05$). This supports the validity of the model, even for lateral offsets that are a significant fraction of the side length of the coils. Note that, despite the moderate deviations from the

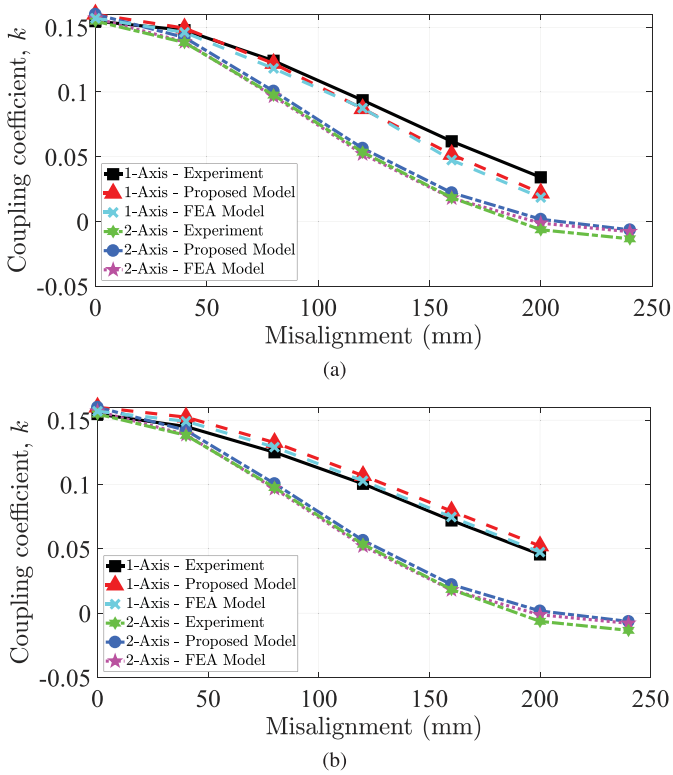

Fig. 20. Coupling coefficient k for lateral offsets in one and two dimensions for rectangular coils. (a) x-axis misalignment. (b) y-axis misalignment.

experiment found in all cases, the relative errors tend to become large in the very low range of coupling factors. This is not a sign of model malfunction; it is rather a consequence of expressing the deviations by means of relative errors.

The three remaining sets of measurements were taken for the rectangular coils. The third and fourth sets correspond to lateral offsets x_0 and y_0 ranging from 0 to 200 mm along the x and y axes, respectively. The fifth set was obtained from simultaneous (x_0, y_0) displacements measured from (0, 0) to (240, 240) mm. This represents a 94.5% of the outer side length of the coils along the x-axis, and a 74.5% along the y-axis. The air gap h was set to 115 mm.

The results are shown in Fig. 20. Note that the 2-D case is repeated in Fig. 20(a) and (b) along with the two corresponding 1-D misalignments for convenience, since this representation facilitates the interpretation of the results: it follows from the plots that k decreases faster when the misalignment occurs along the axis corresponding to the shortest coil side [see Fig. 20(a)]. The threshold for negative values of k is reached around 200 mm for the 2-D misalignment, falling well below zero for the extra values taken at 240 mm. As regards the relative errors, they are 5.68% for a two-axis misalignment of 120 mm ($k > 0.05$) and 20.57% for 160 mm ($k < 0.05$).

IX. Model Performance Under Different Coil Arrangements

The experimental validation for the analytical model carried out in Section VIII was restricted to a magnetic coupler of square

TABLE IX
LIST OF PARAMETRIC STUDIES WITH THE SET OF CHOSEN VALUES FOR EACH ANALYSIS

Parametric study	a **(mm)**	b **(mm)**	N	h **(mm)**	(x_0,y_0) (mm)	S **(mm^2)**	Ω **(mm)**
A - Side b (large coils)	300	100 – 500	9	100	0	6.28	2.83
B - Side b (small coils)	20	10 – 50	8	50	0	0.20	0.50
C - Number of turns N	300	450	5 – 20	100	0	6.28	2.83
D - Air gap h	300	450	9	50 – 250	0	6.28	2.83
E - Misalignment (x_0 , y_0)	300	450	9	100	0 – 200	6.28	2.83

geometry. This section investigates further the accuracy of the model under a number of different rectangular arrangements with the aid of some extra FEA models, especially constructed for extending the scope of validation. Each of the proposed parametric studies focuses on the variation of a single geometrical feature: coil side length, number of turns, air gap, and in-plane misalignment. Furthermore, the variation of the side length is analyzed for both large and small coils, in an attempt to cover the whole range of sizes that can be encountered in the numerous applications of IPT systems, from EV wireless charging to radio frequency identification technology. The set of values chosen to carry out all the parametric studies is gathered together in Table IX.

Unlike the experimental validation, in which the measured coupling coefficient was the parameter selected to characterize the strength of the magnetic coupling, in this article, the parameter chosen to assess the accuracy of the model is the mutual inductance, which is provided by both the analytical and the FEA model.

Fig. 21 shows the self- and mutual-inductance values obtained with both the proposed model and the FEA simulation tool for the parametric study A (variation of side length for large coils). The deviation found for the self-inductance is below 15 μH in all cases except for $b = 100$ mm. This reveals that the accuracy of the proposed model is compromised mainly for short coil lengths. However, the behavior of the proposed model is considerably better in the case of the mutual inductance, since the predictions are very accurate in the whole range of side lengths considered: the largest deviation in this case, that corresponds to $b = 500$ mm, is 0.8 μH.

Similar results are obtained in the parametric study B (variation of side length for small coils). As can be seen in Fig. 22, the agreement is better for the mutual inductance than for the self-inductance. Overall, the deviations are slightly larger for small coils than for large coils.

The influence of the number of turns is analyzed in the parametric study C. Again, the deviations are larger for the self-inductance than for the mutual inductance in the range of coil turns under study. In this case, the deviations show an increasing trend with the number of turns for both the self- and the mutual inductance (see Fig. 23).

The comparison that results from the parametric study D (variation of air gap) is represented in Fig. 24. Note that

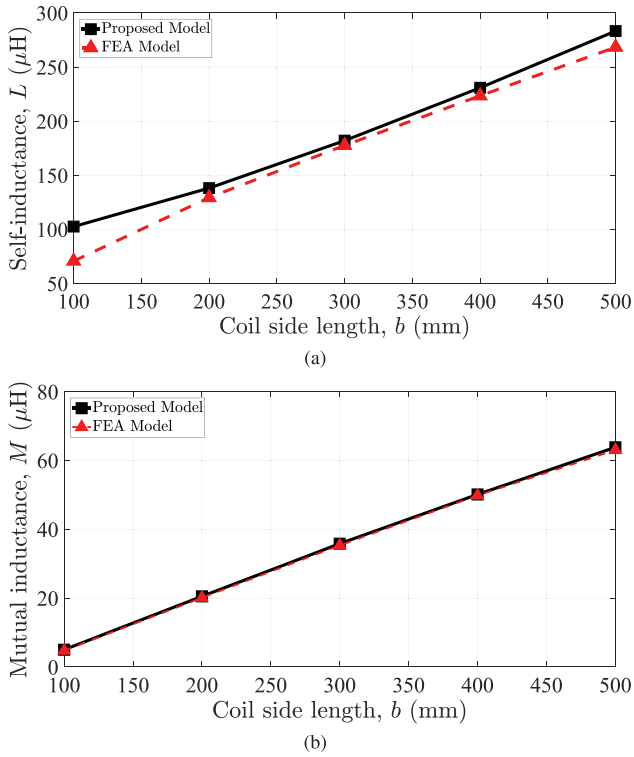

Fig. 21. Parametric study A (see Table IX): Predicted values for (a) self- and (b) mutual inductances.

changes in the air gap affect only the mutual inductance, while the self-inductance remains unaltered. The corresponding self-inductance values for the selected coil dimensions are 256.62 and 245.78 μH, computed with the proposed model and the FEA tool, respectively. The absolute error amounts thus to 10.84 μH. It is apparent from the results that the prediction of the proposed model is rather accurate, regardless of the air gap. The deviations are always below 1.2 μH, which corresponds for an air gap of $h = 50$ mm.

Finally, the influence of a variable in-plane misalignment is considered in the parametric study E. The coil geometry is the same as in the previous study. As can be seen in Fig. 25, the predictions of the proposed model are rather accurate in the whole range of 2-D offsets.

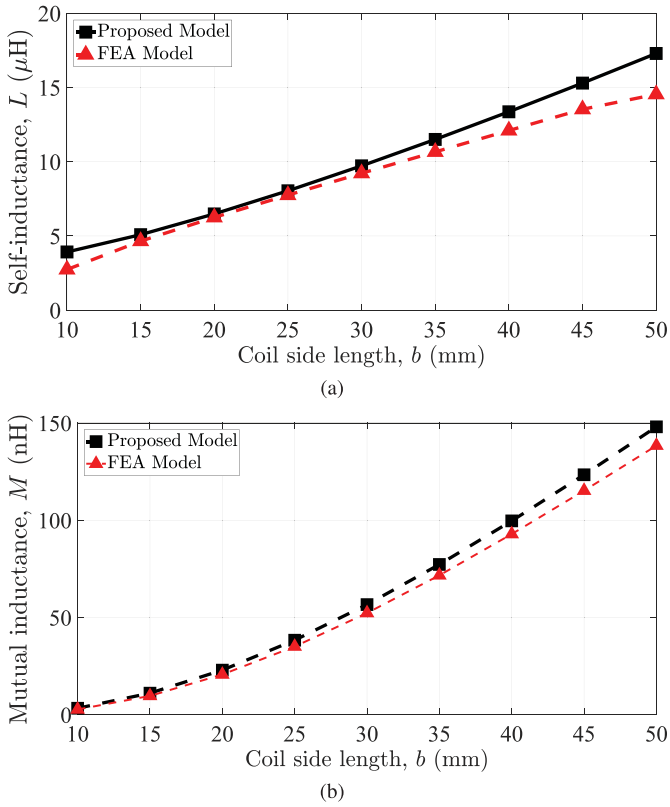

Fig. 22. Parametric study B (see Table IX): Predicted values for (a) self- and (b) mutual inductances.

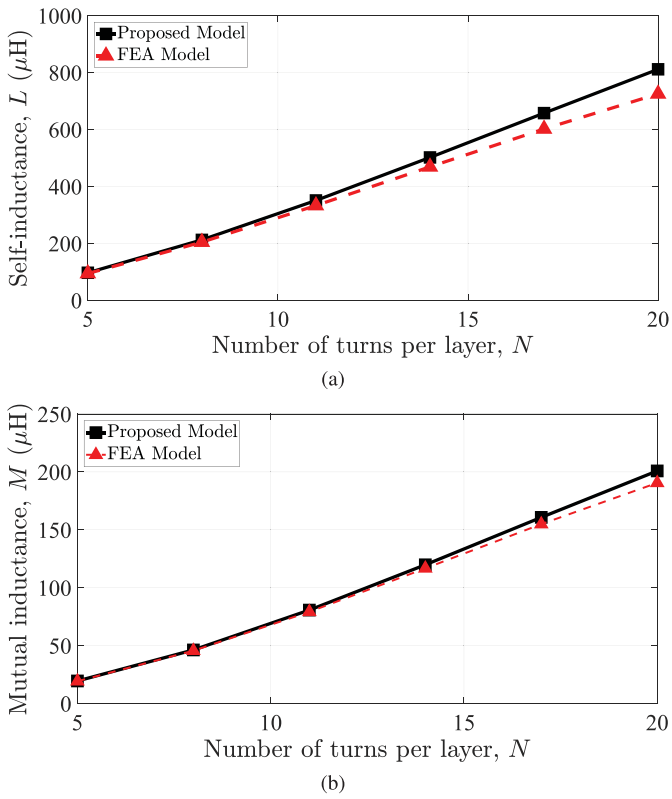

Fig. 23. Parametric study C (see Table IX): Predicted values for (a) self- and (b) mutual inductances.

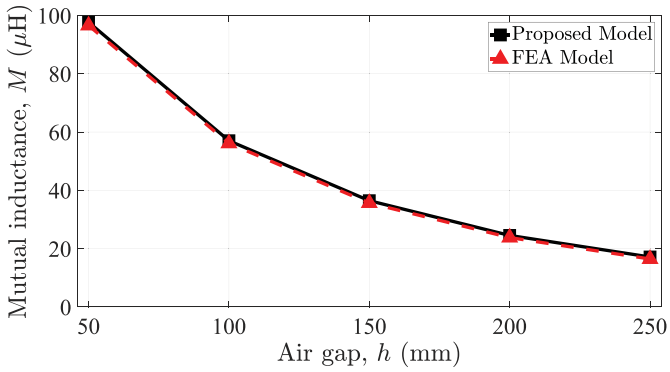

Fig. 24. Parametric study D (see Table IX): Predicted values for the mutual inductance.

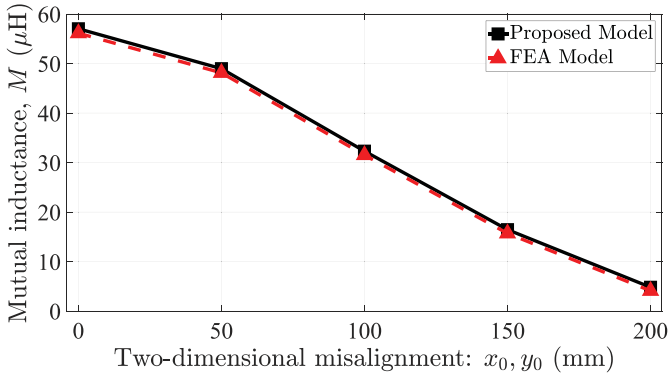

Fig. 25. Parametric study E (see Table IX): Predicted values for the mutual inductance.

X. Key Strengths of the Proposed Model

As mentioned in the introduction, a number of works have already approached the problem of the magnetic interaction between two mutually coupled coils with an air core from different perspectives and varied geometries, most of them in the context of the wireless transfer of power. This section summarizes the strengths of the proposed model in terms of the following aspects: simplicity of the formulation, accuracy in comparison with both experimental results and FEA simulations, and time of execution.

Unlike other models, which rely on integral expressions or complex transformations, the equations involved in the proposed model can be solved by computing simple operations such as logarithms and square roots, which allows the model to be easily programmed without the need of additional libraries or algorithms.

The behavior of the model has proved satisfactory for a wide range of geometrical arrangements. The deviations found from both the experimental results and the FEA simulations are within reasonable limits in all cases. Previous works by other authors have shown similar correlations between experimental and predicted values [18], [19], [25]. Furthermore, the closeness of agreement between the proposed and the FEA model allows us to regard them as complementary software tools. The

TABLE X
EXECUTION TIME OF THE MODEL AND FEA TOOL (EMS) CORRESPONDING TO THE EXPERIMENTAL SQUARE COILS SEPARATED BY 125 mm

Coil arrangements	Time	Method
Self-inductance	2.26 ms	Proposed model
Mutual inductance (aligned coils)	6.74 ms	Proposed model
Mutual inductance (two-dimensional misalignment)	7.38 ms	Proposed model
Mutual inductance (aligned coils)	15 min. 34 s	FEA tool (EMS)
Mutual inductance (two-dimensional misalignment)	18 min. 10 s	FEA tool (EMS)

deviations found between both models in the calculation of self-inductances, though moderate, are somewhat larger than in the case of the mutual inductance.

The execution times achieved with the proposed model, even in the case of running a parametric analysis, are usually in the range of milliseconds. Computational times in the same order of magnitude were reported in [18] and [25]. Simulation results delivered by optimized FEA models require much longer times, in the order of several minutes or even hours. The computer utilized in this work is characterized by an Intel i7 CPU with a clock rate of 3.40 GHz, 8 GB of RAM, and a SATA 3 hard disk drive. Some examples of execution times running the proposed model and the EMS FEA tool are shown in Table X for illustration purposes. These values refer to the models constructed as a replica of the experimental square coils for a separation h equal to 125 mm.

Owing to its fast execution times, the proposed model can contribute to speed up the design process during its early stages, when the sizing and the main geometrical features of the magnetic coupler are still to be defined. At a later stage, CAD tools can provide a complementary characterization of magnetic couplers based on, for example, a thermal analysis or the magnetic flux distribution around the coils.

The comparison between simulation and proposed models shows that the deviation in the calculation of self-inductance is higher than in mutual inductance. However, the deviations are lower enough to think that proposed and simulation models can complement each other. Due to its lower execution time, proposed model can assist the FEA tool by the realization of a parametric analysis during its early stages, when the sizing and the main geometrical features of the magnetic coupler are still to be defined. At a later stage, CAD tools can provide a complementary characterization of magnetic couplers based on, for example, a thermal analysis or the magnetic flux distribution around the coils.

XI. CONCLUSION

This article provides a thorough description of an analytical model whose objective is the accurate calculation of the self-inductances and the mutual inductance of two mutually coupled rectangular coils. The model considers all the individual interactions present among the different turns, and the simplifications made are limited to the calculations performed on the corners of the coils.

These coils on which the model was built are equal, parallel, share a planar geometry, and feature either one or two equal layers of turns per coil. For comparison purposes, an alternative simplified model that relies on the reduction of the coupled coils to equivalent single-turn coils was also tested for the particular case of coaxial square-shaped coils. The proposed model was experimentally validated by means of measurements performed on both square and rectangular magnetic couplers.

The comparison of the results provided by the proposed model with the self-inductance and mutual inductance values obtained from experimental measurements taken with an air gap between coils of 125 mm allows us to conclude that there is a noticeable agreement. In the case of the square coupler, the relative errors found for that air gap amount to 3.38% for the self-inductance L_1 (worst case) and to 1.76% for the mutual inductance, while in the rectangular coupler these errors are 6.00% and 1.39%, respectively. The model also behaved satisfactorily for other air gaps in the range of 50–200 mm, as the deviations from the experimental results are small in all cases, particularly in the case of larger air gaps.

The single-turn model also agreed reasonably well with the experiment, but only as regards the mutual inductance calculations, for which the relative error attained was 3.25%. However, the error was above 30% for the two self-inductances. The proposed model, which relies on a more complex formulation than the single-turn model, yielded better results in both cases, which reinforces its reliability.

The behavior of the proposed model when there is some degree of in-plane misalignment between the two coils is also satisfactory. The largest relative errors for the corresponding offsets in one and two dimensions found with the square coils are 3.18% and 6.22%, being 5.69% and 7.00% in the case of the rectangular coils, when k is above 0.05 in both cases.

The extension of the experimental validation carried out with the aid of additional FEA models contributed to support the validity of the proposed model under a number of varied coil arrangements. Overall, the degree of agreement was satisfactory, being always better for the mutual inductance than for the self-inductance calculations.

ACKNOWLEDGMENT

The authors would like to thank EMWORKS for granting the license to use the student version of the electric and magnetic simulation software EMS in this research article.

REFERENCES

[1] P. Li and R. Bashirullah, "A wireless power interface for rechargeable battery operated medical implants," *IEEE Trans. Circuits Syst. II, Express Briefs*, vol. 54, no. 10, pp. 912–916, Oct. 2007.

[2] S. Y. R. Hui and W. W. C. Ho, "A new generation of universal contactless battery charging platform for portable consumer electronic equipment," *IEEE Trans. Power Electron.*, vol. 20, no. 3, pp. 620–627, May 2005.

[3] Z. Bi, T. Kan, C. C. Mi, Y. Zhang, Z. Zhao, and G. A. Keoleian, "A review of wireless power transfer for electric vehicles: Prospects to enhance sustainable mobility," *Appl. Energy*, vol. 179, pp. 413–425, 2016.

[4] S. D. Barman, A. W. Reza, N. Kumar, M. E. Karim, and A. B. Munir, "Wireless powering by magnetic resonant coupling: Recent trends in wireless power transfer system and its applications," *Renew. Sustain. Energy Rev.*, vol. 51, pp. 1525–1552, 2015.

[5] D. Liu, H. Hu, and S. V. Georgakopoulos, "Misalignment sensitivity of strongly coupled wireless power transfer systems," *IEEE Trans. Power Electron.*, vol. 32, no. 7, pp. 5509–5519, Jul. 2017.

[6] R. Bosshard and J. W. Kolar, "Multi-objective optimization of 50 kW/85 kHz IPT system for public transport," *IEEE J. Emerg. Sel. Topics Power Electron.*, vol. 4, no. 4, pp. 1370–1382, Dec. 2016.

[7] J. Kim *et al.*, "Coil design and shielding methods for a magnetic resonant wireless power transfer system," *Proc. IEEE*, vol. 101, no. 6, pp. 1332–1342, Jun. 2013.

[8] Y. Yang, M. El Baghdadi, Y. Lan, Y. Benomar, J. Van Mierlo, and O. Hegazy, "Design methodology, modeling, and comparative study of wireless power transfer systems for electric vehicles," *Energies*, vol. 11, no. 7, 2018, Art. no. 1716.

[9] R. Bosshard, J. W. Kolar, and B. Wunsch, "Accurate finite-element modeling and experimental verification of inductive power transfer coil design," in *Proc. 29th Appl. Power Electron. Conf. Expo.*, 2014, pp. 1648–1653.

[10] R. Bosshard, U. Iruretagoyena, and J. W. Kolar, "Comprehensive evaluation of rectangular and double-D coil geometry for 50 kW/85 kHz IPT system," *IEEE J. Emerg. Sel. Topics Power Electron.*, vol. 4, no. 4, pp. 1406–1415, Dec. 2016.

[11] M. T. Thompson, "Inductance calculation techniques—Part II: Approximations and handbook methods," *Power Control Intell. Motion*, 1991.

[12] H. A. Wheeler, "Inductance formulas for circular and square coils," *Proc. IEEE*, vol. 70, no. 12, pp. 1449–1450, Dec. 1982.

[13] W. G. Hurley *et al.*, "A unified approach to the calculation of self-and mutual-inductance for coaxial coils in air," *IEEE Trans. Power Electron.*, vol. 30, no. 11, pp. 6155–6162, Nov. 2015.

[14] M. Bueno and A. Assis, "Equivalence between the formulas for inductance calculation," *Can. J. Phys.*, vol. 75, no. 6, pp. 357–362, 1997.

[15] M. A. Bueno and A. K. T. Assis, "A new method for inductance calculations," *J. Phys. D: Appl. Phys.*, vol. 28, no. 9, pp. 1802–1806, 1995.

[16] Z. Luo and X. Wei, "Analysis of square and circular planar spiral coils in wireless power transfer system for electric vehicles," *IEEE Trans. Ind. Electron.*, vol. 65, no. 1, pp. 331–341, Jan. 2018.

[17] F. W. Grover, *Formulas and Tables for the Calculation of the Inductance of Coils of Polygonal Form*. Washington, DC, USA: U.S. Dept. Commerce, Bureau of Standards, 1922.

[18] W. Dehui, S. Qisheng, W. Xiaohong, and Y. Fan, "Analytical model of mutual coupling between rectangular spiral coils with lateral misalignment for wireless power applications," *IET Power Electron.*, vol. 11, no. 5, pp. 781–786, May 2018.

[19] S. Raju, R. Wu, M. Chan, and C. P. Yue, "Modeling of mutual coupling between planar inductors in wireless power applications," *IEEE Trans. Power Electron*, vol. 29, no. 1, pp. 481–490, Jan. 2014.

[20] M. Soma, D. C. Galbraith, and R. L. White, "Radio-frequency coils in implantable devices: Misalignment analysis and design procedure," *IEEE Trans. Biomed. Eng.*, vol. BME-34, no. 4, pp. 276–282, Apr. 1987.

[21] K. Fotopoulou and B. W. Flynn, "Wireless power transfer in loosely coupled links: Coil misalignment model," *IEEE Trans. Magn.*, vol. 47, no. 2, pp. 416–430, Feb. 2011.

[22] E. B. Rosa, "The self and mutual inductances of linear conductors," *Bull. Bureau Standards*, vol. 4, no. 2, pp. 301–344, 1908.

[23] F. W. Grover, *Inductance Calculations*. New York, NY, USA: Van Nostrand, 1946.

[24] H. Greenhouse, "Design of planar rectangular microelectronic inductors," *IEEE Trans. Parts, Hybrids, Packag.*, vol. PHP-10, no. 2, pp. 101–109, Jun. 1974.

[25] S. R. Khan, S. K. Pavuluri, and M. P. Y. Desmulliez, "Accurate modeling of coil inductance for near-field wireless power transfer," *IEEE Trans. Microw. Theory Techn.*, vol. 66, no. 9, pp. 4158–4169, Sep. 2018.

[26] Z. Luo and X. Wei, "Mutual inductance analysis of planar coils with misalignment for wireless power transfer systems in electric vehicle," in *Proc. IEEE Veh. Power Propulsion Conf.*, Oct. 2016, pp. 1–6.

[27] Y. Gao, C. Duan, A. A. Oliveira, A. Ginart, K. B. Farley, and Z. T. H. Tse, "3-D coil positioning based on magnetic sensing for wireless EV charging," *IEEE Trans. Transp. Electrific.*, vol. 3, no. 3, pp. 578–588, Sep. 2017.

[28] J. Vázquez, P. Roncero-Sánchez, and A. P. Torres, "Coupling factor of a weak inductive coupling in a 2-kW power transfer system with a 125-mm air gap for electric vehicle chargers," in *Proc. IEEE 26th Int. Symp. Ind. Electron.*, Jun. 2017, pp. 670–675.

[29] J. Vázquez, P. Roncero-Sánchez, and A. P. Torres, "An inductive power transfer system for the wireless charging of electric vehicles: Determination of the magnetic coupling factor," in *Emerging Capabilities and Applications of Wireless Power Transfer*. Hershey, PA, USA: IGI Global, 2019, pp. 292–322.

[30] X. d. T. García, J. Vázquez, and P. Roncero-Sánchez, "Design, implementation issues and performance of an inductive power transfer system for electric vehicle chargers with series–series compensation," *IET Power Electron.*, vol. 8, no. 10, pp. 1920–1930, 2015.

[31] J. Vázquez, P. Roncero-Sánchez, and A. Parreño Torres, "Simulation model of a 2-kW IPT charger with phase-shift control: Validation through the tuning of the coupling factor," *Electron.*, vol. 7, no. 10, 2018, Art. no. 255.

[32] C. R. Paul, *Introduction to Electromagnetic Compatibility*. Hoboken, NJ, USA: Wiley, 2006.

[33] B. Hesterman, "Analysis and modeling of magnetic coupling," Denver Chapter, IEEE Power Electron. Soc., 2007, pp. 15–19.

[34] R. Bosshard, J. W. Kolar, J. Mühlethaler, I. Stevanović, B. Wunsch, and F. Canales, "Modeling and $\eta - \alpha$-Pareto optimization of inductive power transfer coils for electric vehicles," *IEEE J. Emerg. Sel. Topics Power Electron.*, vol. 3, no. 1, pp. 50–64, Mar. 2015.

[35] R. Bosshard, J. Mühlethaler, J. W. Kolar, and I. Stevanović, "Optimized magnetic design for inductive power transfer coils," in *Proc. 28th Annu. IEEE Appl. Power Electron. Conf. Expo.*, Mar. 2013, pp. 1812–1819.

[36] Z. Li, C. Zhu, J. Jiang, K. Song, and G. Wei, "A 3-kW wireless power transfer system for sightseeing car supercapacitor charge," *IEEE Trans. Power Electron.*, vol. 32, no. 5, pp. 3301–3316, May 2017.

[37] P. Tan, C. Liu, L. Ye, and T. Peng, "Modeling and experimentation of multi-coil switching coupler for wireless power transfer systems," in *Proc. IEEE Energy Convers. Congr. Expo.*, Oct. 2017, pp. 2579–2583.

[38] C. Liu, S. Ge, Y. Guo, H. Li, and G. Cai, "Double-LCL resonant compensation network for electric vehicles wireless power transfer: Experimental study and analysis," *IET Power Electron.*, vol. 9, no. 11, pp. 2262–2270, 2016.

[39] J. Acero, C. Carretero, I. Lope, R. Alonso, O. Lucia, and J. M. Burdio, "Analysis of the mutual inductance of planar-lumped inductive power transfer systems," *IEEE Trans. Ind. Electron.*, vol. 60, no. 1, pp. 410–420, Jan. 2013.

Francisco Javier López-Alcolea (Member, IEEE) received the four-year bachelor's degree in industrial electronics and control engineering from the University of Castilla–La Mancha, Ciudad Real, Spain, in 2017. He is currently working toward the master's degree with a focus on research in electrical, electronics, and industrial control engineering with the Universidad Nacional de Educación a Distancia, Madrid, Spain.

He is currently a Researcher with the University of Castilla–La Mancha. His current research interests include wireless power transfer systems, control, and power electronics.

Javier Vázquez del Real received the M.Sc. degree in physics from the University of Valencia, Valencia, Spain, in 1992, the master's degree in telecommunications from the Polytechnic University of Madrid, Madrid, Spain, in 2001, and the Ph.D. degree from the University of Castilla–La Mancha, Ciudad Real, Spain, in 2006.

After obtaining predoctoral grants to work with the Research Centre for Optoelectronic Devices, Alcatel, Stuttgart, Germany, and with the Valencian Institute for Agricultural Research, Valencia, he held engineering positions in multinational corporations, such as Bosch and Valeo. In 2001, he joined the University of Castilla–La Mancha, where he is currently a Lecturer in electronics. He has participated in postdoctoral visits to Newcastle University, Newcastle upon Tyne, U.K., and to the IK4-Research Alliance, Basque Country, Spain. His research interests include power electronics and sensors.

Pedro Roncero-Sánchez (SM'14) received the Ph.D. degree in industrial engineering from the University of Castilla–La Mancha, Ciudad Real, Spain, in 2004.

From 2006 to the end of 2007, he carried out postdoctoral research with the University of Glasgow, Glasgow, U.K., in the field of the control of power electronic converters for the amelioration of power quality. Since 2012, he has been an Associate Professor with the School of Industrial Engineering, University of Castilla–La Mancha, where he conducts several R&D projects. His research interests include the control of power electronic converters, power quality, renewable energy systems, energy storage devices, and wireless power transfer systems.

Alfonso Parreño Torres received the M.Sc. degree in electronic engineering from the University of Valencia, Valencia, Spain, in 2006, and the Ph.D. degree from the University of Castilla–La Mancha, Ciudad Real, Spain, in 2016.

He is currently with the Castilla–La Mancha Science and Technology Park, Albacete, Spain, and with the University of Castilla–La Mancha as a Part-Time Assistant Professor. His research interests include control, power electronics, power quality, and signal processing algorithms for electrical power systems.